Pseudospectral and Runge-Kutta-Nyström methods for second-order wave equations: Stable and accurate boundary treatments

Chun-Hao Teng[a,*], Misun Min[b], Juen-Kai Wang[c,d]

[a] *Department of Applied Mathematics and Center of Mathematical Modeling and Scientific Computing, National Chiao Tung University, Hsinchu, Taiwan 30010*
[b] *Mathematics and Computer Science Division, Argonne National Laboratory, Argonne, IL 60439, USA*
[c] *Center for Condensed Matter Sciences, National Taiwan University, Taipei, Taiwan 106*
[d] *Institute of Atomic and Molecular Sciences, Academia Sinica, Taipei, Taiwan*

Abstract

In this study we propose pseudospectral schemes for second-order wave equations subject to general boundary conditions, including Dirichlet, Neumann, Robin, and materials interface conditions. The boundary conditions are enforced in the schemes through a penalty method, and special attention is paid to analyzing the stability of the schemes. In addition we discuss how to consistently impose boundary conditions at the intermediate stages of the Runge-Kutta-Nyström method, to avoid order reduction. The proposed schemes can be used in multidomain computational frameworks for simulating wave problems on complex domains. Numerical validations are conducted, and the expected convergence is observed.

Keywords: spectral/pseudospectral methods, penalty boundary conditions, second-order wave equations.

1. Introduction

Many wave phenomena in general relativity, acoustics, elastodynamics, and electrodynamics are described by second-order wave equations. By introducing auxiliary variables these second-order wave equations in many cases can be rewritten as equivalent first-order systems of equations. For example, in elastodynamics the stress-displacement equations can be rewritten as stress-velocity equations. As pointed out in [27] the advantage of performing simulations based on first-order equations is that many numerical stability issues related to first-order systems of equations have been addressed because of the mature development of computational fluid dynamics. However, this order reduction approach has a drawback. It increases the total number of equations to be solved and thus increases the computational load.

In wave simulations the problem domains may be large compared with the wavelength. Thus, simulating a wave propagating for a long distance implies a long time integration. Consequently, the simulation quality

*Corresponding author
Email addresses: `tengch@math.nctu.edu.tw` (Chun-Hao Teng), `mmin@mcs.anl.gov` (Misun Min), `jkwang@ntu.edu.tw` (Juen-Kai Wang)

may be affected because of the accumulation of numerical dispersion errors. High-order methods have been shown to be more efficient than low-order methods in preserving low accumulation of dispersion errors during long time integrations, especially for multidimensional space problems [26]. Since the 1990s many high-order schemes have been developed for simulating large-scale wave problems.

In addition to the large domain issue, simulating waves in regions involving heterogeneous media is important. To accurately model wave phenomena at materials interfaces, one must specify suitable boundary conditions to relate field values on both sides of the interface. However, imposing boundary conditions in numerical partial differential equations is delicate [13]. Generally speaking, great care must be taken to construct consistent and stable boundary closures for high-order schemes in order to ensure accurate modeling of wave dynamics at materials interfaces.

Many high-order schemes have been devised for complex wave simulations based on first-order systems of equations. Here, we briefly discuss some high-order schemes for wave equations in second-order form. A class of high-order difference schemes, satisfying certain summation-by-parts rules, has been constructed for scalar wave equations [28–32], elastic wave equations [3, 6], and Einstein's equations [33]. High-order schemes based on spectral-element and multidomain pseudospectral methods have been designed for second-order evolution equations [12, 25, 35], elastic wave equations [2, 7, 24, 39], and Einstein's equations [37]. Discontinuous Galerkin finite-element methods have also been employed to devise schemes for acoustic wave equations [1, 4, 16], Maxwell's equations [17], and Einstein's equations [8].

In this study we present high-order schemes for second-order wave equations in one- and two-dimensional spaces. Our approach is based on the Legendre pseudospectral method [21, 23] in space and the Runge-Kutta-Nyström (RKN) algorithm [34] in time. In the present schemes primitive boundary conditions are enforced weakly through a penalty method [10, 11]. Special attention is paid to analyzing the stability of these schemes subject to Dirichlet, Neumann, Robin, and materials interface boundary conditions. Through conducting energy estimates we show that the proposed schemes can be made stable by properly choosing the values of the penalty parameters. We use one- and two-dimensional space problems to illustrate the ideas of our method in detail. In addition to the stable boundary treatments in space, we propose an approach for consistently imposing time-dependent boundary conditions at the intermediate stages of the RKN method, to avoid order reduction. The basic schemes can be used in a multidomain computational framework, similar to the approaches in [9, 20, 22, 38], to solve wave equations in complex domains. Indeed, we have conducted numerical experiments for wave problems in one- and two-dimensional spaces, and we have observed the expected convergence results.

The rest of the paper is organized as follows. In Section 2 we present the schemes for the second-order wave equations, and we discuss boundary treatments to ensure the stability and accuracy of the schemes. Section 3 is devoted to the numerical validation of the methods for wave problems in one- and two-dimensional spaces. Concluding remarks are given in Section 4.

2. Formulations

In this section we introduce numerical schemes for one- and two-dimensional second-order waves and we discuss boundary treatments of these schemes to ensure stability and accuracy.

2.1. Model 1D problems

Denote as (x,t) the space-time coordinate. Let $\mathsf{D}^{(1)} = [x_L, 0]$ and $\mathsf{D}^{(2)} = [0, x_R]$. We consider $u^{(\nu)}(x,t)$ for $\nu = 1,2$ satisfying the initial boundary value problem (IBVP):

$$\ddot{u}^{(\nu)}(x,t) = a^{(\nu)}(x)\left(b^{(\nu)}(x)u'(x,t)\right)', \qquad x \in \mathsf{D}^{(\nu)}, \quad t > 0, \tag{1a}$$

$$u^{(\nu)}(x,0) = f^{(\nu)}(x), \quad \dot{u}^{(\nu)}(x,0) = h^{(\nu)}(x), \qquad x \in \mathsf{D}^{(\nu)}, \tag{1b}$$

$$\mathcal{B}_L u^{(1)}(x_L,t) = g_L(t), \quad \mathcal{B}_L = \alpha_L - \beta_L \partial_x, \qquad t > 0, \tag{1c}$$

$$\mathcal{B}_R u^{(2)}(x_R,t) = g_R(t), \quad \mathcal{B}_R = \alpha_R + \beta_R \partial_x, \qquad t > 0, \tag{1d}$$

$$u^{(1)}(0,t) = u^{(2)}(0,t), \qquad t > 0, \tag{1e}$$

$$b^{(1)}(0)\partial_x u^{(1)}(0,t) = b^{(2)}(0)\partial_x u^{(2)}(0,t), \qquad t > 0. \tag{1f}$$

The symbol $\cdot$ denotes the time differentiation, and $' = \partial_x$ denotes the differentiation with respect to the space argument. For $\nu = 1,2$, $a^{(\nu)}(x) > 0$ and $b^{(\nu)}(x) > 0$ are assumed smooth functions, and $f^{(\nu)}$ and $h^{(\nu)}$ are the initial data of $u^{(\nu)}$ and $\dot{u}^{(\nu)}$, respectively. $\mathcal{B}_L u^{(1)} = g_L(t)$ and $\mathcal{B}_R u^{(2)} = g_R(t)$ are the boundary conditions applied at the end points x_L and x_R, respectively. $\mathcal{B}_L$ and $\mathcal{B}_R$ are termed boundary operators, and they are parameterized by non-negative real numbers, α_L, β_L, α_R, and β_R. Equations (1e)–(1f) are the interface boundary conditions relating field values on both sides of the interface at $x = 0$. For homogeneous boundary conditions, $g_L = g_R = 0$, the problem leads to an energy estimate

$$\begin{aligned}\sum_{\nu=1}^{2}\int_{\mathsf{D}^{(\nu)}} \frac{(\dot{u}^{(\nu)})^2}{a^{(\nu)}} + b^{(\nu)}(\partial_x u^{(\nu)})^2\,dx \le \sum_{\nu=1}^{2}\int_{\mathsf{D}^{(\nu)}} \frac{(h^{(\nu)})^2}{a^{(\nu)}} + b^{(\nu)}(\partial_x f^{(\nu)})^2 dx \\ + \frac{\alpha_L}{\beta_L}\left(b^{(1)}(f^{(1)})^2\right)\Big|_{x_L} + \frac{\alpha_R}{\beta_R}\left(b^{(2)}(f^{(2)})^2\right)\Big|_{x_R},\end{aligned} \tag{2}$$

provided that $\alpha_L/\beta_L \ge 0$ and $\alpha_R/\beta_R \ge 0$.

2.2. Pseudospectral methods for 1D wave equations

We now present stable boundary treatments for one-dimensional pseudospectral schemes for second-order wave equations.

2.2.1. Legendre pseudospectral method

Let N be a positive integer and $\mathsf{I} = [-1,1]$. Denote as $\boldsymbol{\xi} = \{\xi_i\}_{i=0}^{N}$ the set of Legendre-Gauss-Lobatto (LGL) grid points on I. These points are roots of the polynomial $(1-\xi^2)P_N'(\xi)$, where $P_N(\xi)$ is the Nth-degree Legendre polynomial. We adopt the Legendre pseudospectral method to approximate a function $u(\xi)$

and its derivative defined on I as follows,

$$u(\xi) \approx \mathcal{I}_N u(\xi) = \sum_{j=0}^{N} l_j(\xi) u(\xi_j), \quad u'(\xi) \approx (\mathcal{I}_N u(\xi))' = \sum_{j=0}^{N} l_j'(\xi) u(\xi_j),$$

where $\mathcal{I}_N$ is the interpolation operator and $l_j(\xi) = -\frac{(1-\xi^2)P_N'(\xi)}{N(N+1)(\xi-\xi_j)P_N(\xi_j)}$ for $j = 0, 1, ..., N$ are the Lagrange basis polynomials based on the LGL grid points, satisfying $l_j(\xi_i) = \delta_{ij}$, with δ_{ij} being the usual Kronecker delta function. Associated with a set of LGL points is a set of quadrature weights, denoted by $\boldsymbol{\omega} = \{\omega_i\}_{i=0}^N$, and we have the quadrature integration formula

$$\int_{\mathsf{I}} f(\xi)\, d\xi = \sum_{i=0}^{N} f(\xi_i)\omega_i, \tag{3}$$

provided that $f(\xi)$ is a polynomial with degree at most $2N - 1$.

To apply the approximation method for functions defined on a general interval, say, $\mathsf{D} = [x_L, x_R]$, we introduce a coordinate transformation to map I onto D. For simplicity and without losing generality, we consider a linear coordinate mapping $x(\xi)$ and its inverse $\xi(x)$ as

$$x(\xi) = x_L + J(\xi + 1), \quad \xi(x) = -1 + (x - x_L)/J, \quad J = (x_R - x_L)/2,$$

with J being the Jacobian of the mapping. Then, we can approximate $u(x)$ and $u'(x)$ defined on D as

$$u(x) \approx \mathcal{I}_N u(x) = \sum_{j=0}^{N} L_j(x) u(x_j), \quad u'(x) \approx (\mathcal{I}_N u(x))' = \sum_{j=0}^{N} L_j'(x) u(x_j),$$

where $L_j(x) = l_j(\xi(x))$, $L_j'(x) = l_j'(\xi)/J$, and $x_j = x(\xi_j)$ for $j = 0, 1, ..., N$ are the LGL grid points on D. The integration quadrature rule, Eq. (3), through coordinate transformation becomes

$$\int_{\mathsf{D}} u(x) dx = \sum_{i=0}^{N} u(x_i) J\omega_i, \tag{4}$$

provided that u is a polynomial with degree at most $2N - 1$. We have the following rules based on the quadrature formula for further use. Let u and v be polynomials of degree at most N. So, uv' and $u'v$ are polynomials of degree at most $2N - 1$. Then,

$$\sum_{i=0}^{N} J\omega_i u(x_i) v'(x_i) = u(x_N)v(x_N) - u(x_0)v(x_0) - \sum_{i=0}^{N} J\omega_i u'(x_i) v(x_i), \tag{5a}$$

$$\sum_{i=0}^{N} J\omega_i u(x_i) (\mathcal{I}_N(v(x)L_j(x)))'\big|_{x_i} = u(x_N)v(x_N)\delta_{jN} - u(x_0)v(x_0)\delta_{j0} - J\omega_j v(x_j) u'(x_j). \tag{5b}$$

Equation (5a) is a summation-by-parts rule mimicking the integration-by-parts formula. It is obtained from converting the summation by its integral representation, performing integration by parts, and then rewriting the resultant integral by its equivalent discrete summation. Equation (5b) is obtained by substituting $v'(x) = (\mathcal{I}_N(v(x)L_j(x)))'$ into Eq. (5a) and then employing $L_j(x_i) = \delta_{ij}$.

For further details of the Legendre pseudospectral method we refer the reader to [23].

2.2.2. Basic scheme and stable boundary treatments

We now discuss stable boundary treatments at $x = x_L$ and $x = x_R$ described by Eqs. (1c)–(1d). For simplicity we omit the subscript (ν) in Eqs. (1a)–(1d) and consider $u(x,t)$, $x \in \mathsf{D} = [x_L, x_R]$, satisfying Eqs. (1a)-(1d). To numerically solve the problem by Legendre pseudospectral method on the interval D, we collocate $N+1$ LGL grid points, x_j for $j = 0, 1, ..., N$ and denote the field values at the grid points by $v_j(t)$. We seek a numerical solution of the form

$$v(x,t) = \sum_{j=0}^{N} L_j(x) v_j(t),$$

satisfying the collocation equations

$$\begin{aligned}\frac{1}{a_i}\ddot{v}_i =& (b_i v_i' - b_i L_N(x_i)\tau_R(\mathcal{B}_R v_N - g_R) + b_i L_0(x_i)\tau_L(\mathcal{B}_L v_0 - g_L))' \\ &- \frac{\sigma_R b_N}{J\omega_N} L_N(x_i)(\mathcal{B}_R v_N - g_R), -\frac{\sigma_R b_0}{J\omega_0} L_0(x_i)(\mathcal{B}_L v_0 - g_L), \qquad i = 0, 1, ..., N, \qquad (6a)\\ v_i =& f_i, \quad \dot{v}_i = h_i, \qquad i = 0, 1, ..., N, \qquad (6b)\end{aligned}$$

where we have used $a_i = a(x_i)$, $b_i = b_i(x_i)$, $f_i = f(x_i)$, and $h_i = h(x_i)$, and where τ_L, τ_R, σ_L, and σ_R are penalty parameters whose values will be determined later to ensure the stability of the scheme.

We now conduct a stability analysis. It is sufficient to consider homogeneous boundary conditions, namely, $g_L = g_R = 0$. Multiplying $\dot{v}_i J\omega_i$ to Eq. (6a) and summing the resultants, we have

$$\begin{aligned}\frac{1}{2}\frac{d}{dt}\sum_{i=0}^{N}\frac{\dot{v}_i^2}{a_i}J\omega_i =& \sum_{i=0}^{N} J\omega_i \dot{v}_i (b_i v_i')' - \tau_R(\mathcal{B}_R v_N)\sum_{i=0}^{N} J\omega_i \dot{v}_i (b_i L_N(x_i))' + \tau_L(\mathcal{B}_L v_0)\sum_{i=0}^{N} J\omega_i \dot{v}_i (b_i L_0(x_i))' \\ &- \sigma_R b_N \dot{v}_N (\mathcal{B}_R v_N) - \sigma_L b_0 (\dot{v}_0)(\mathcal{B}_L v_0). \qquad (7)\end{aligned}$$

Let us focus on the first summation term on the right-hand side of Eq. (7). We notice that $\dot{v}_i(b_i v_i')'$ are the values of the polynomial $\dot{v}(x,t)(\mathcal{I}_N[b(x)v'(x,t)])'$ at the grid points. Since $\dot{v}(\mathcal{I}_N[bv'])'$ is a polynomial of degree $2N-1$, we invoke Eq. (5a) and obtain

$$\sum_{i=0}^{N} J\omega_i \dot{v}_i (b_i v_i')' = b_N \dot{v}_N v_N' - b_0 \dot{v}_0 v_0' - J\omega_0 b_0 \dot{v}_0' v_0' - J\omega_N b_N \dot{v}_N' v_N' - \frac{1}{2}\frac{d}{dt}\sum_{i=1}^{N-1} J\omega_i b_i (v_i')^2. \qquad (8)$$

Following a similar argument, we apply Eq. (5b) to evaluate the other two summation terms on the right-hand side of Eq. (7). The results are

$$-\tau_R(\mathcal{B}_R v_N)\sum_{i=0}^{N} J\omega_i \dot{v}_i (b_i L_N(x_i))' = -\tau_R(\alpha_R v_N + \beta_R v_N')(b_N \dot{v}_N - J\omega_N b_N \dot{v}_N'), \qquad (9)$$

$$\tau_L(\mathcal{B}_L v_0)\sum_{i=0}^{N} J\omega_i \dot{v}_i (b_i L_0(x_i))' = \tau_L(\alpha_L v_0 - \beta_L v_0')(-b_0 \dot{v}_0 - J\omega_0 b_0 \dot{v}_0'). \qquad (10)$$

Substituting Eqs. (8)–(10) into Eq. (7), we obtain an energy rate equation

$$\dot{E} = 2\dot{\boldsymbol{r}}_L^T \boldsymbol{M}_L \boldsymbol{r}_L + 2\dot{\boldsymbol{r}}_L^T \boldsymbol{M}_R \boldsymbol{r}_R, \tag{11}$$

where E is the energy defined as

$$E = \sum_{i=0}^{N} J\omega_i b_i (v_i')^2 + \sum_{i=1}^{N-1} J\omega_i b_i (v_i')^2 + \left(1 - c^{-1}\right) J\omega_0 b_0 (v_0')^2 + \left(1 - c^{-1}\right) J\omega_N b_N (v_N')^2, \quad c \geq 1,$$

$\boldsymbol{r}_L$ and $\boldsymbol{r}_R$ are vectors given as $\boldsymbol{r}_L(t) = \sqrt{b_0}[v_0,\, -v_0']^T$ and $\boldsymbol{r}_R(t) = \sqrt{b_N}[v_N,\, v_N']^T$, where the superscript T denotes the vector transpose, and $\boldsymbol{M}_L$ and $\boldsymbol{M}_R$ are matrices given explicitly as

$$\boldsymbol{M} = \begin{bmatrix} -\alpha(\tau+\sigma) & 1 - \beta(\tau+\sigma) \\ \alpha\tau J\omega & -(1/c - \beta\tau)J\omega \end{bmatrix}, \quad \omega = \frac{2}{N(N+1)}. \tag{12}$$

We have omitted the associated subscripts L and R for clarity. As suggested in [30–32], if we can choose the values of the penalty parameters τ and σ such that $\boldsymbol{M}$ is symmetric semi-negative definite, then we have $2\dot{\boldsymbol{r}}^T \boldsymbol{M} \boldsymbol{r} = d(\boldsymbol{r}^T \boldsymbol{M} \boldsymbol{r})/dt$. As a consequence, integrating Eq. (11) with respect to t and employing the symmetric semi-negative definite property of $\boldsymbol{M}$, we arrive at a bounded energy estimate of

$$E(t) \leq E(0) - (\boldsymbol{r}_L^T \boldsymbol{M}_L \boldsymbol{r}_L)|_{t=0} - (\boldsymbol{r}_R^T \boldsymbol{M}_R \boldsymbol{r}_R)|_{t=0},$$

implying the stability of the scheme.

We now provide a set of penalty parameters such that $\boldsymbol{M}$ is symmetric semi-negative definite. Let

$$\tau = \frac{1}{\alpha J\omega + (1 + \gamma(c-1))\beta}, \quad \sigma = \gamma(c-1)\tau, \quad \gamma \geq 1, \tag{13}$$

where γ is termed the penalty strength parameter. Then, $\boldsymbol{M}$ becomes symmetric:

$$\boldsymbol{M} = \begin{bmatrix} -\alpha\tau(1+\gamma(c-1)) & \alpha\tau J\omega \\ \alpha\tau J\omega & -c^{-1} J\omega\tau(\alpha J\omega + \beta(c-1)(\gamma-1)) \end{bmatrix}.$$

Denoted by $\mu = \mu_1$ and $\mu = \mu_2$, the eigenvalues of $\boldsymbol{M}$ satisfy the characteristic equation

$$\mu^2 + p\mu + q = 0, \quad \text{with} \quad \begin{cases} p = (\alpha(1+\gamma(c-1)) + c^{-1}(\alpha J\omega + \beta(c-1)(\gamma-1))J\omega)\tau \\ q = c^{-1}\alpha\tau(\gamma-1)(c-1)J\omega \end{cases}.$$

Notice that $-p = \mu_1 + \mu_2$ and $q = \mu_1\mu_2$. Hence, for $c \geq 1$ and $\gamma \geq 1$ we have $-p \leq 0$ and $q \geq 0$, indicating that both μ_1 and μ_2 are nonpositive. We conclude that $\boldsymbol{M}$ is semi-negative definite.

Before proceeding further we comment on the present way of imposing boundary conditions.

Comment 1. In order to ensure the stability of the scheme Eq. (6), it is sufficient to consider $c = 1$, which leads to $\sigma = 0$. This approach leads to penalizing boundary conditions at every collocation equation. If the boundary condition to be enforced is of Neumann or Robin type, one can alternatively take $\tau = 0$ and

$\sigma = 1/\beta$, and the resulting matrix $\boldsymbol{M}$ deduced from Eq. (12) is also symmetric semi-negative definite. For this case the penalized boundary conditions are introduced only to the two end-point collocation equations. However, as we will see soon from the eigen-spectrum analysis, the latter approach leads to a smaller time step for stable computations when an explicit time-marching scheme is used, and this is a drawback.

Comment 2. The reason for considering $c \neq 1$, particularly for $c = 2$ and $c = 3$, is the following. The stability analysis for the one-dimensional scheme has led to a matrix $\boldsymbol{M}$ associated with an end point, and for stable computations we need to make the matrix $\boldsymbol{M}$ symmetric semi-negative definite, by providing suitable values of τ and σ. We will soon show that for two-dimensional problems a similar energy analysis leads to a family of matrices associated with domain boundary grid points, and the $\boldsymbol{M}$ matrix associated with a quadrilateral vertex is similar to the matrix $\boldsymbol{M}$ given in Eq. (12) with $c = 2$.

Comment 3. In this study we impose boundary conditions in the primitivity form. For first-order hyperbolic systems of equations it is preferred to impose characteristic boundary conditions as suggested in [13]. For second-order hyperbolic wave equations well-posed characteristic boundary conditions [18, 19] have been derived, and the theory has been applied to construct a pseudospectral scheme for simulating black-hole activities [37]. The differences between imposing characteristic and primitivity boundary conditions require further investigation.

2.2.3. Eigenvalue spectra and penalty parameters

For homogeneous boundary conditions, Eq. (6a) leads to a system of second-order ordinary differential equations with a general solution as follows:

$$\ddot{\boldsymbol{u}}(t) = \mathcal{L}\boldsymbol{u}(t), \quad \boldsymbol{u} = \sum_{i=0}^{N} \boldsymbol{\zeta}_i \exp(\sqrt{\lambda_i}\, t), \tag{14}$$

where $\boldsymbol{u}(t) = [u_0(t), u_1(t), ..., u_N(t)]^T$, $\mathcal{L}$ is a matrix operator resulting from the right-hand side expression of Eq. (6a), and λ_i and $\boldsymbol{\zeta}_i$ are the eigenvalues and the associated eigenvectors of the matrix operator $\mathcal{L}$, respectively.

We have shown that the scheme has a bounded energy estimate. This indicates that all the eigenvalues of $\mathcal{L}$ are real and nonpositive, which can be validated by calculating the eigenvalues of $\mathcal{L}$. Figure 1 presents the eigenvalue spectra of $\mathcal{L}$ for boundary conditions imposed at both end points being of the same type (both Dirichlet or both Neumann), for various values of N. The penalty parameters τ and σ are given by Eq. (13) with $c = 1$ and $\gamma = 1$. Indeed, the results show that the eigenvalues of $\mathcal{L}$ are real and semi-negative.

Later, we will use the Runge-Kutta-Nyström method to advance numerical solutions in time. To maintain stable computations, we require some knowledge of the spectral radius of the matrix $\mathcal{L}$, denoted by $\rho(\mathcal{L})$, as a function of N. Here we consider only the matrix operators $\mathcal{L}$ resulting from Eq. (6) with boundary conditions imposed at both end points being of the same type. The $\mathcal{L}$ operators corresponding to Dirichlet,

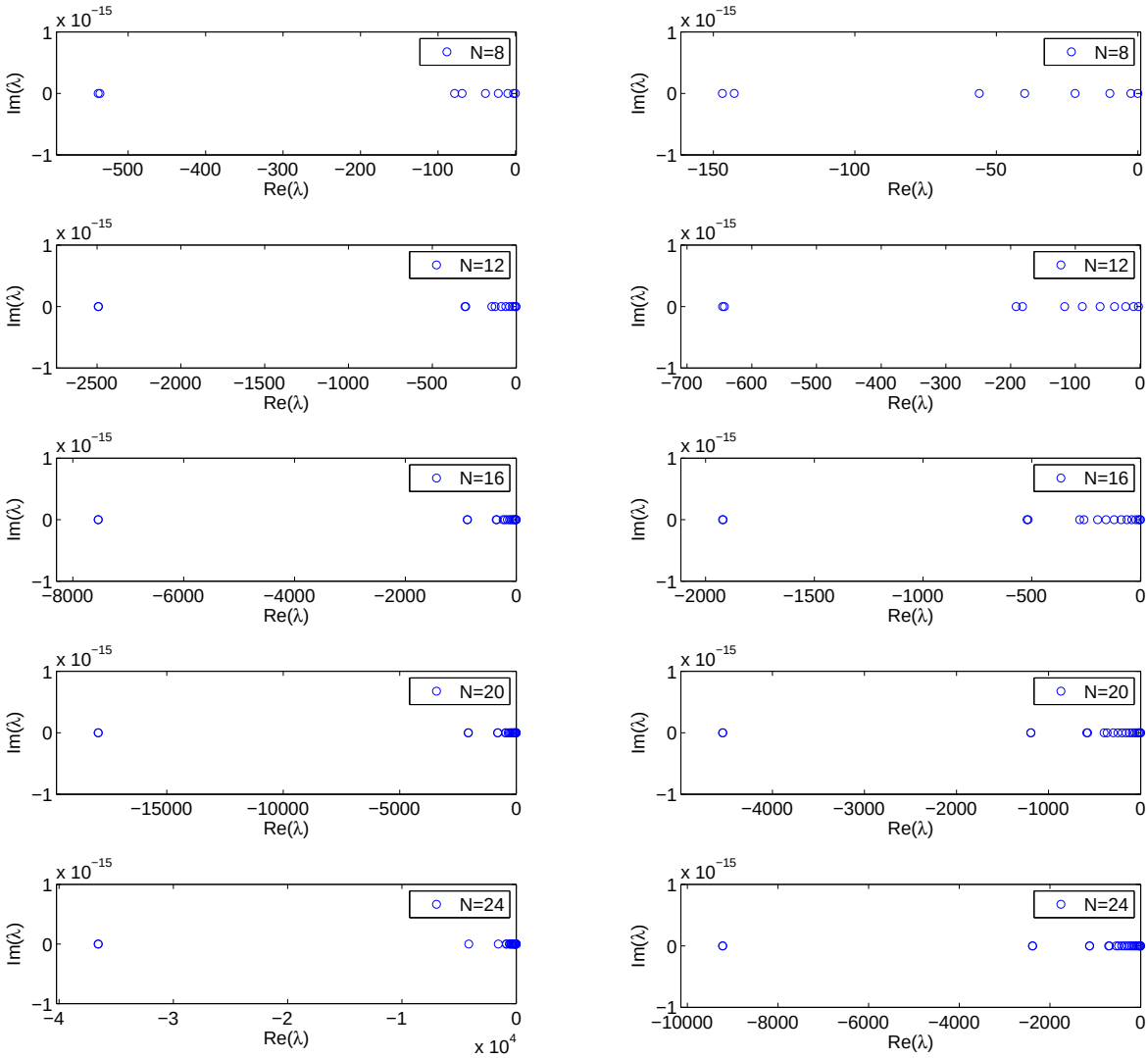

Figure 1: Eigenvalue spectra of $\mathcal{L}$ corresponding to Dirichlet (left column) and Neumann (right column) boundary conditions applied at both end points, for various values of N.

Neumann, and two Robin cases parameterized by $(\alpha, \beta) = (1, 0.1)$ and $(\alpha, \beta) = (1, 0.01)$ are investigated in this study. The square root of the spectral radius of $\mathcal{L}$ is designated as $\Lambda(\mathcal{L})$, that is, $\Lambda = \sqrt{\rho(\mathcal{L})}$. We are interested in how the penalty parameters, τ and σ, affect $\Lambda(\mathcal{L})$. Notice that τ and σ in Eq. (13) involve other parameters, $c \geq 1$ and $\gamma \geq 1$. Here we use c and γ to characterize τ and σ, and we calculate $\Lambda(\mathcal{L})$ as a function of N. For convenience, these discrete values are plotted and connected as a curve, termed the Λ-curve of $\mathcal{L}$.

Figure 2(a) presents the Λ-curves of the $\mathcal{L}$ operators corresponding to the Dirichlet, Neumann, and two Robin cases, for $c = 1$ and $\gamma = 1$. The results show that the two Robin case curves lie between the Dirichlet

case curve and the Neumann case curve and that for both the Dirichlet and Neumann cases, $\Lambda(\mathcal{L})$ grows quadratically as N increases. In addition, for each N the value of the Neumann case $\Lambda(\mathcal{L})$ is smaller than that of the Dirichlet case $\Lambda(\mathcal{L})$ approximately by a factor of 2. We therefore will use the Dirichlet case $\Lambda(\mathcal{L})$ as a conservative guideline to estimate stable time steps of $\mathcal{O}(N^{-2})$.

In Fig. 2(b) we present the Λ-curves corresponding to the Neumann and two Robin cases, for $\tau = 0$ and $\sigma = 1/\beta$. For this set of penalty parameters only the Neumann or Robin condition can be imposed, and the penalized boundary conditions appear only at the two end collocation equations. The figure shows that the Neumann case Λ-curve also scales like N^2. For a given N, however, the value of the Neumann case $\Lambda(\mathcal{L})$ shown in Fig. 2(b) is larger than that of the Neumann case $\Lambda(\mathcal{L})$ shown in Fig. 2(a), approximately by a factor of 2. We therefore will not consider using $\tau = 0$ and $\sigma = 1/\beta$ to enforce boundary conditions because this set of parameters results in a smaller time step for stable computations.

In Fig. 2(c) and Fig. 2(e) we present the Λ-curves of the considered $\mathcal{L}$ operators using $(c, \gamma) = (2, 1)$ and $(c, \gamma) = (3, 1)$, respectively. Considering the curves in Fig. 2(a) as a reference, we observe that the Λ-curves move upward as the value of c increases. These results indicate that increasing the value of c increases the stiffness of the $\mathcal{L}$ operator and thus reduces the maximum stable time step. However, we cannot avoid using $c > 1$ for multidimensional space problems, as will be shown later. Hence, we use $c = 1$ whenever possible.

Figures 2(d) and 2(f) present the Λ-curves of the considered $\mathcal{L}$ operators using $(c, \gamma) = (2, 2)$ and $(c, \gamma) = (3, 2)$, respectively. Compared with the curves shown in Fig. 2(c) and Fig. 2(e), the Λ-curves also move upward as the value of γ increases. This result similar to the situation of increasing the value of c. Hence, we use $\gamma = 1$ whenever possible.

2.2.4. Two-domain scheme and penalty interface boundary condition

We now discuss an approach for imposing interface boundary conditions. Let us return to the IBVP described by Eqs. (1a)–(1f). Notice that the interface boundary conditions Eqs. (1e)-(1f) can be rewritten as expressions similar to Eqs. (1c)–(1d), by introducing the following interface boundary operators and the associated boundary constraints on both sides of the interface $x = 0$:

$$\text{on } \mathsf{D}^{(1)} \text{ side} \quad \mathcal{B}v^{(1)}|_{x=0^-} = \left[v^{(1)} + \beta^{(1)} b^{(1)} \left(v^{(1)}\right)'\right]\Big|_{x=0^-}, \quad g = \left[v^{(2)} + \beta^{(1)} b^{(2)} \left(v^{(2)}\right)'\right]\Big|_{x=0^+}, \tag{15a}$$

$$\text{on } \mathsf{D}^{(2)} \text{ side} \quad \mathcal{B}v^{(2)}|_{x=0^+} = \left[v^{(2)} - \beta^{(2)} b^{(2)} \left(v^{(2)}\right)'\right]\Big|_{x=0^+}, \quad g = \left[v^{(1)} - \beta^{(2)} b^{(1)} \left(v^{(1)}\right)'\right]\Big|_{x=0^-}, \tag{15b}$$

where $\beta^{(1)}$ and $\beta^{(2)}$ are positive real numbers whose values will be determined later in the stability analysis. In the above expressions, the interface boundary conditions are simply linear combinations Eqs. (1e) and (1f) parameterized by $\beta^{(1)}$ and $\beta^{(2)}$, which can be viewed as defining Robin-type boundary operators and suitable boundary functions on both sides of the interface.

We now present the scheme for the problem described by Eqs. (1a)–(1f). We introduce linear coordinate mapping functions to map $\mathsf{D}^{(\nu)}$ onto I. The corresponding Jacobian of the coordinate transformations are

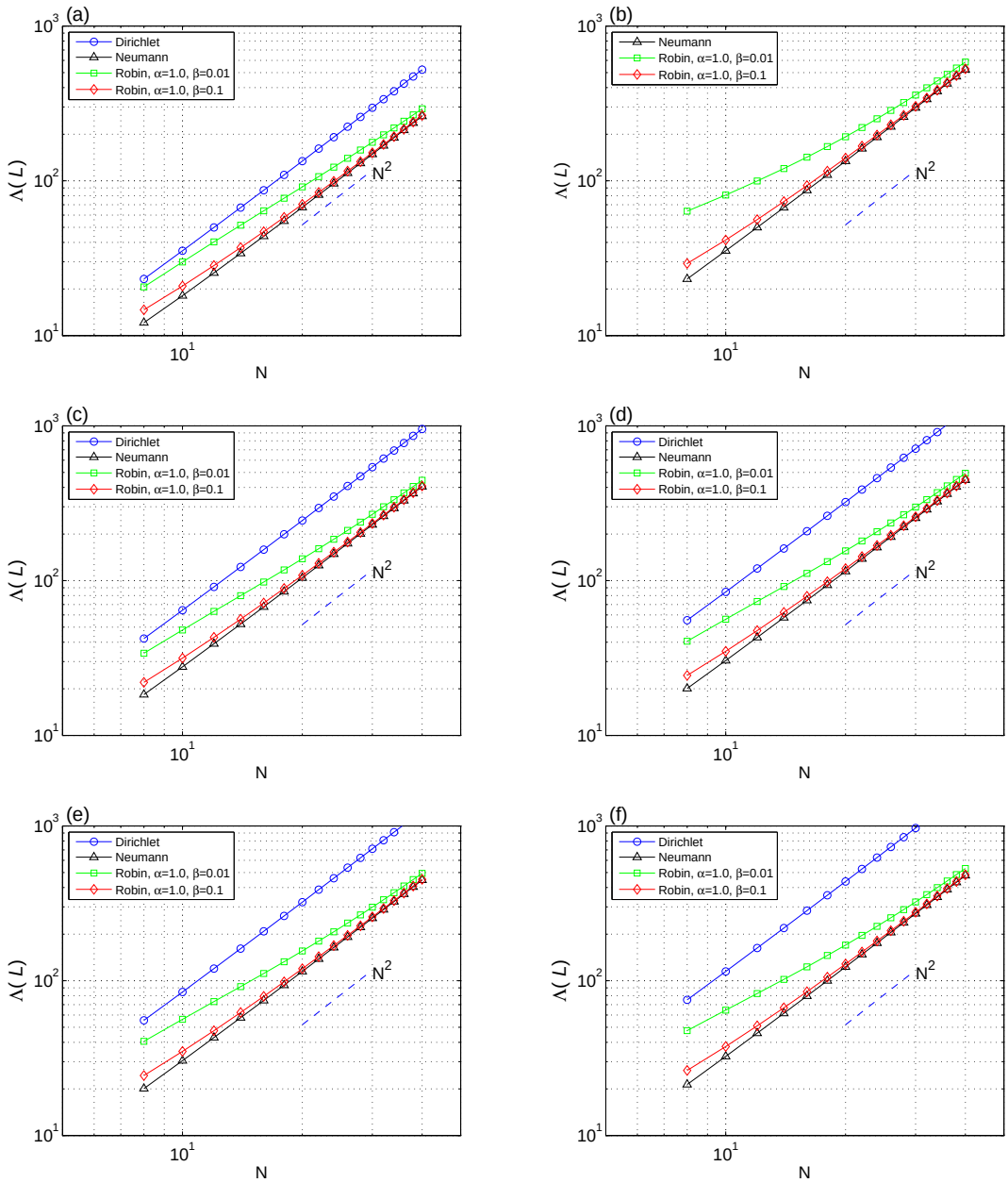

Figure 2: Square roots of the spectral radii of $\mathcal{L}$ as functions of N. The penalty parameters τ and σ are computed by Eq. (13) using different values of c and γ. (a): $(c, \gamma) = (1, 1)$. (b): $\tau = 0$, $\sigma = 1/\beta$. (c): $(c, \gamma) = (2, 1)$. (d): $(c, \gamma) = (2, 2)$. (e): $(c, \gamma) = (3, 1)$. (f): $(c, \gamma) = (3, 2)$.

denoted by $J^{(\nu)}$. On $\mathsf{D}^{(\nu)}$ we collocate $N^{(\nu)} + 1$ LGL grid points, $x_j^{(\nu)}$ for $j = 0, 1, ..., N^{(\nu)}$. The associated quadrature weights and the Lagrange basis polynomials are denoted by $\omega_i^{(\nu)}$ and $L_i^{(\nu)}(x^{(\nu)})$, respectively, for

$0 \le i \le N^{(\nu)}$. We seek numerical solutions $v^{(\nu)}$ for $\nu = 1, 2$ of the form

$$v^{(\nu)}(x^{(\nu)}, t) = \sum_{j=0}^{N^{(\nu)}} L_j^{(\nu)}(x^{(\nu)}) v_j^{(\nu)}(t), \tag{16}$$

satisfying the collocation equations

$$\begin{aligned}\frac{\ddot{v}_i^{(1)}}{a_i^{(1)}} =& \left(b_i^{(1)}(v_i^{(1)})'\right)' - \tau^{(1)}\left(b_i^{(1)} L_{N^{(1)}}^{(1)}(x_i^{(1)})\right)'\left(\left(v_{N^{(1)}}^{(1)} - v_0^{(2)}\right) + \beta^{(1)}\left(b_{N^{(1)}}^{(1)}(v_{N^{(1)}}^{(1)})' - b_0^{(2)}(v_0^{(2)})'\right)\right) \\ &- \frac{\sigma^{(1)} b_{N^{(1)}}^{(1)} L_{N^{(1)}}^{(1)}(x_i^{(1)})}{J^{(1)}\omega_{N^{(1)}}^{(1)}}\left(\left(v_{N^{(1)}}^{(1)} - v_0^{(2)}\right) + \beta^{(1)}\left(b_{N^{(1)}}^{(1)}(v_{N^{(1)}}^{(1)})' - b_0^{(2)}(v_0^{(2)})'\right)\right), \quad i = 0, ..., N^{(1)}\end{aligned} \tag{17a}$$

$$\begin{aligned}\frac{\ddot{v}_i^{(2)}}{a_i^{(2)}} =& \left(b_i^{(2)}(v_i^{(2)})'\right)' + \tau^{(2)}\left(b_i^{(2)} L_0^{(2)}(x_i^{(2)})\right)'\left(\left(v_0^{(2)} - v_{N^{(1)}}^{(1)}\right) - \beta^{(2)}\left(b_0^{(2)}(v_0^{(2)})' - b_{N^{(1)}}^{(1)}(v_{N^{(1)}}^{(1)})'\right)\right) \\ &- \frac{\sigma^{(2)} b_0^{(2)} L_0^{(2)}(x_i^{(2)})}{J^{(2)}\omega_0^{(2)}}\left(\left(v_0^{(2)} - v_{N^{(1)}}^{(1)}\right) - \beta^{(2)}\left(b_0^{(2)}(v_0^{(2)})' - b_{N^{(1)}}^{(1)}(v_{N^{(1)}}^{(1)})'\right)\right), \quad i = 0, ..., N^{(2)}\end{aligned} \tag{17b}$$

$$v_i^{(\nu)}(0) = f_i^{(\nu)}, \quad \dot{v}_i^{(\nu)}(0) = h_i^{(\nu)}, \quad i = 0, 1, ..., N^{(\nu)}. \tag{17c}$$

Because the boundary conditions at the outer boundaries are enforced in the same way as in Eq. (6a), we have omitted them for clarity.

We now focus on determining suitable values of $\beta^{(\nu)}$, $\tau^{(\nu)}$, and $\sigma^{(\nu)}$, such that the scheme is stable. Multiplying $\dot{v}_i^{(1)} J^{(1)}\omega_i^{(1)}$ and $\dot{v}_i^{(2)} J^{(2)}\omega_i^{(2)}$ to Eq. (17a) and Eq. (17b), respectively, summing the resultants, invoking the quadrature rules, and conducting integration by parts, we obtain an energy rate equation:

$$\dot{E}(t) = 2\dot{\boldsymbol{r}}^T \boldsymbol{M} \boldsymbol{r},$$

where $E(t)$ is the energy defined as

$$\begin{aligned}E(t) =& \sum_{\nu=1}^{2}\left(\sum_{i=0}^{N^{(\nu)}} \frac{(\dot{v}_i^{(\nu)})^2}{a_i^{(\nu)}} J^{(\nu)}\omega_i^{(\nu)} + \sum_{i=1}^{N^{(\nu)}-1} b_i^{(\nu)}((v_i^{(\nu)})')^2 J^{(\nu)}\omega_i^{(\nu)}\right) \\ &+ \left(1 - c^{-1}\right) b_{N^{(1)}}^{(1)}\left((v_{N^{(1)}}^{(1)})'\right)^2 J^{(1)}\omega_{N^{(1)}}^{(1)} + \left(1 - c^{-1}\right) b_0^{(2)}\left((v_0^{(2)})'\right)^2 J^{(2)}\omega_0^{(2)}, \quad c \ge 1,\end{aligned}$$

$\boldsymbol{r}$ is a vector defined as $\boldsymbol{r} = \left[v_{N^{(1)}}^{(1)},\, v_0^{(2)},\, b_{N^{(1)}}^{(1)}(v_{N^{(1)}}^{(1)})',\, b_0^{(2)}(v_0^{(2)})'\right]^T$, and $\boldsymbol{M}$ is a matrix given as

$$\boldsymbol{M} = \begin{bmatrix} -\widetilde{\tau}^{(1)} b^{(1)} & \widetilde{\tau}^{(1)} b^{(1)} & 1 - \widetilde{\tau}^{(1)}\beta^{(1)} b^{(1)} & \widetilde{\tau}^{(1)}\beta^{(1)} b^{(1)} \\ \widetilde{\tau}^{(2)} b^{(2)} & -\widetilde{\tau}^{(2)} b^{(2)} & -\widetilde{\tau}^{(2)}\beta^{(2)} b^{(2)} & -(1 - \widetilde{\tau}^{(2)}\beta^{(2)} b^{(2)}) \\ \tau^{(1)}\bar{\omega}^{(1)} & -\tau^{(1)}\bar{\omega}^{(1)} & -(1/(cb^{(1)}) - \tau^{(1)}\beta^{(1)})\bar{\omega}^{(1)} & -\tau^{(1)}\bar{\omega}^{(1)}\beta^{(1)} \\ \tau^{(2)}\bar{\omega}^{(2)} & -\tau^{(2)}\bar{\omega}^{(2)} & -\tau^{(2)}\beta^{(2)}\bar{\omega}^{(2)} & -(1/(cb^{(2)}) - \tau^{(2)}\beta^{(2)})\bar{\omega}^{(2)} \end{bmatrix}, \tag{18}$$

with

$$\widetilde{\tau}^{(\nu)} = \tau^{(\nu)} + \sigma^{(\nu)}, \quad \bar{\omega}^{(\nu)} = \frac{2J^{(\nu)}}{N^{(\nu)}(N^{(\nu)} + 1)}, \quad \nu = 1, 2.$$

To ensure stable imposition of the interface boundary conditions, we seek suitable values of $\beta^{(\nu)}$, $\tau^{(\nu)}$, and $\sigma^{(\nu)}$ such that the matrix $\boldsymbol{M}$ is symmetric semi-negative definite. Let

$$\beta^{(1)} = \frac{\bar{\omega}^{(2)}}{(1+\gamma(c-1))b^{(2)}}, \quad \tau^{(1)} = \frac{b^{(2)}}{b^{(2)}\bar{\omega}^{(1)} + b^{(1)}\bar{\omega}^{(2)}}, \quad \sigma^{(1)} = \gamma(c-1)\tau^{(1)}, \quad \gamma \geq 1$$
$$\beta^{(2)} = \frac{\bar{\omega}^{(1)}}{(1+\gamma(c-1))b^{(1)}}, \quad \tau^{(2)} = \frac{b^{(1)}}{b^{(2)}\bar{\omega}^{(1)} + b^{(1)}\bar{\omega}^{(2)}}, \quad \sigma^{(2)} = \gamma(c-1)\tau^{(2)}, \quad \gamma \geq 1.$$

Then $\boldsymbol{M}$ becomes symmetric as

$$\boldsymbol{M} = m \begin{bmatrix} -1 & 1 & \beta^{(2)} & \beta^{(1)} \\ 1 & -1 & -\beta^{(2)} & -\beta^{(1)} \\ \beta^{(2)} & -\beta^{(2)} & -(d_1\beta^{(2)} + d_2\beta^{(1)})\beta^{(2)} & -\beta^{(1)}\beta^{(2)} \\ \beta^{(1)} & -\beta^{(1)} & -\beta^{(1)}\beta^{(2)} & -(d_1\beta^{(1)} + d_2\beta^{(2)})\beta^{(1)} \end{bmatrix}, \tag{19}$$

with

$$m = \frac{(1+\gamma(c-1))b^{(1)}b^{(2)}}{b^{(2)}\bar{\omega}^{(1)} + b^{(1)}\bar{\omega}^{(2)}}, \quad d_1 = \frac{1+\gamma(c-1)}{c}, \quad d_2 = \frac{(\gamma-1)(c-1)}{c}.$$

We claim that the eigenvalues of $\boldsymbol{M}$ are nonpositive for $\gamma \geq 1$ and $c \geq 1$. This fact can be verified through examining the signs of the eigenvalues of $m^{-1}\boldsymbol{M}$ instead, since $m > 0$. The eigenvalues of $m^{-1}\boldsymbol{M}$ satisfy the characteristic equation

$$\mu(\mu^3 + A\mu^2 + B\mu + C) = 0,$$

with

$$A = 2 + \sum_{\nu=1}^{2}(\beta^{(\nu)})^2 + d_2\left(\sum_{\nu=1}^{2}\beta^{(\nu)}\right)^2, \quad B = d_2\left(\sum_{\nu=1}^{2}\beta^{(\nu)}\right)^2(2 + d_1\beta^{(1)}\beta^{(2)}), \quad C = 2d_2\beta^{(1)}\beta^{(2)}\left(\sum_{\nu=1}^{2}\beta^{(\nu)}\right)^2.$$

We immediately know that 0 is an eigenvalue and the other three eigenvalues satisfy the cubic polynomial. Notice that for $\gamma \geq 1$ and $c \geq 1$ the parameters $\beta^{(1)}$, $\beta^{(2)}$, d_1, and d_2 are positive. Consequently, the coefficients A, B, and C in the cubic polynomials are non-negative. Employing Descartes' rule of signs we conclude that the cubic polynomial has no positive roots. Therefore, $\boldsymbol{M}$ is symmetric semi-negative definite, and we obtain an energy estimate

$$E(t) \leq E(0) - (\boldsymbol{r}\boldsymbol{M}\boldsymbol{r})|_{t=0},$$

implying that the scheme is stable.

2.3. Multidimensional scheme

We now construct a scheme for wave equations for two-dimensional space problems.

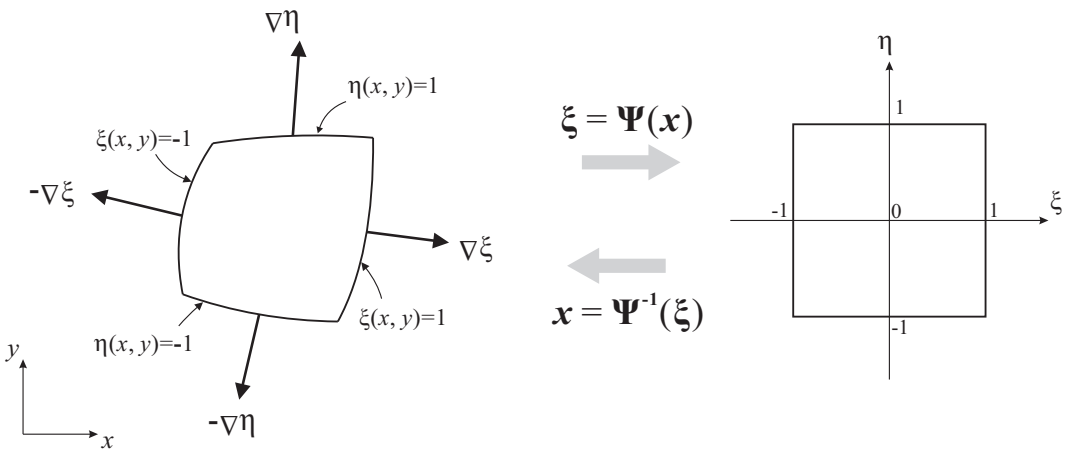

Figure 3: Mapping of a domain Ω smoothly mapped onto $\mathsf{I}^2 = [-1, 1]^2$.

2.3.1. Treatment for exterior boundary conditions

Denote as $\boldsymbol{x} = (x, y)$ and t the space and time coordinates, respectively. Without losing generality consider a domain Ω that can be mapped onto a square domain $\mathsf{I}^2 = [-1, 1]^2$ with a coordinate system termed $\boldsymbol{\xi} = (\xi, \eta)$, as shown in Fig. 3. Consider $u(\boldsymbol{x}, t)$ satisfying the IBVP:

$$\ddot{u}(\boldsymbol{x}, t) = a(\boldsymbol{x})\nabla \cdot (b(\boldsymbol{x})\nabla u(\boldsymbol{x}, t)), \qquad \boldsymbol{x} \in \Omega, \quad t > 0, \tag{20a}$$

$$u(\boldsymbol{x}, 0) = f(\boldsymbol{x}), \quad \dot{u}(\boldsymbol{x}, 0) = h(\boldsymbol{x}), \qquad \boldsymbol{x} \in \Omega, \tag{20b}$$

$$\mathcal{B}u(\boldsymbol{x}, t) = \alpha(\boldsymbol{x})u + \beta(\boldsymbol{x})\boldsymbol{n} \cdot \nabla u = g(t), \qquad \boldsymbol{x} \in \partial\Omega, \quad t > 0, \tag{20c}$$

where $a(\boldsymbol{x}) > 0$ and $b(\boldsymbol{x}) > 0$ are smooth functions and $\alpha(\boldsymbol{x}) > 0$ and $\beta(\boldsymbol{x}) > 0$ are functions defined on the domain boundary $\partial\Omega$. For homogeneous boundary conditions the problem leads to an energy estimate

$$\int_\Omega \frac{\dot{u}^2(\boldsymbol{x}, t)}{a(\boldsymbol{x})} + b(\boldsymbol{x})|\nabla u(\boldsymbol{x}, t)|^2 d\boldsymbol{x} \leq \int_\Omega \frac{h^2(\boldsymbol{x})}{a(\boldsymbol{x})} + b(\boldsymbol{x})|\nabla f(\boldsymbol{x})|^2 d\boldsymbol{x} + \oint_\Omega \frac{\alpha(\boldsymbol{x})}{\beta(\boldsymbol{x})} f^2(\boldsymbol{x}) d\boldsymbol{x}.$$

To numerically solve the problem, we first rewrite the problem in a curvilinear coordinate. Employing the transfinite blending method [14, 15], we construct a one-to-one correspondence coordinate transformation, $\boldsymbol{x} = \boldsymbol{x}(\boldsymbol{\xi})$ and its inverse $\boldsymbol{\xi} = \boldsymbol{\xi}(\boldsymbol{x})$, to associate Ω and I^2. The transformation metric variables are related as follows:

$$\frac{\partial \boldsymbol{x}}{\partial \boldsymbol{\xi}} = \begin{bmatrix} \frac{\partial x}{\partial \xi} & \frac{\partial x}{\partial \eta} \\ \frac{\partial y}{\partial \xi} & \frac{\partial y}{\partial \eta} \end{bmatrix}, \quad \frac{\partial \boldsymbol{\xi}}{\partial \boldsymbol{x}} = \begin{bmatrix} \frac{\partial \xi}{\partial x} & \frac{\partial \xi}{\partial y} \\ \frac{\partial \eta}{\partial x} & \frac{\partial \eta}{\partial y} \end{bmatrix}, \quad \frac{\partial \boldsymbol{x}}{\partial \boldsymbol{\xi}} \frac{\partial \boldsymbol{\xi}}{\partial \boldsymbol{x}} = \boldsymbol{I},$$

with $\boldsymbol{I}$ being the identity matrix.

Employing the coordinate mapping, we transform the variables in Eqs. (20a)–(20c). Here we use the expression $u(\xi, \eta, t) = u(\boldsymbol{x}(\boldsymbol{\xi}), t)$ to simplify the notations, and likewise for the other variables, a, b, f, h, α,

and β. The wave equation in the curvilinear coordinate becomes

$$\ddot{u} = \frac{a}{J}\left(\frac{\partial(J\nabla\xi\cdot\widetilde{\boldsymbol{F}})}{\partial\xi} + \frac{\partial(J\nabla\eta\cdot\widetilde{\boldsymbol{F}})}{\partial\eta}\right), \quad \widetilde{\boldsymbol{F}} = b\nabla u = b\left(\nabla\xi\frac{\partial u}{\partial\xi} + \nabla\eta\frac{\partial u}{\partial\eta}\right),$$

where J is the Jacobian of the coordinate transformation.

To solve the problem defined on the square domain I^2, we introduce $M+1$ and $N+1$ LGL grid points, ξ_i for $i = 0, 1, ..., M$ and η_j for $j = 0, 1, ..., N$, along the ξ and η axes, respectively. The quadrature weights associated with the grid points ξ_i and η_j are denoted by ω_i^ξ and ω_j^η, respectively. Based on the grid points ξ_i and η_j, we denote the Lagrange interpolations functions by $l_i^\xi(\xi)$ and $l_j^\eta(\xi)$, respectively. Employing these basis functions and the quadrature weights, we define the two-dimensional quadrature weights and the two-dimensional Lagrange basis polynomials as $\boldsymbol{\omega}_{i,j} = \omega_i^\xi\omega_j^\eta$ and $L_{i,j}(\xi,\eta) = l_i^\xi(\xi)l_j^\eta(\xi)$, respectively.

Let $v_{i,j}(t)$ be the field values at the grid points. We seek an approximation $v(\xi,\eta,t)$ of the form

$$v(\xi,\eta,t) = \sum_{j=0}^{N}\sum_{i=0}^{M} L_{i,j}(\xi,\eta)v_{i,j},$$

satisfying the collocation equations

$$\ddot{v}_{i,j} = \frac{a_{i,j}}{J_{i,j}}\left(\frac{\partial(bJ\nabla\xi\cdot\boldsymbol{F})}{\partial\xi}\Big|_{i,j} + \frac{\partial(bJ\nabla\eta\cdot\boldsymbol{F})}{\partial\eta}\Big|_{i,j} + Q_{i,j}\right), \qquad \begin{array}{l} i = 0,1,...,M, \\ j = 0,1,...,N, \end{array} \tag{21a}$$

$$v_{i,j}(0) = f_{i,j}, \quad \dot{v}_{i,j}(0) = h_{i,j}, \qquad \begin{array}{l} i = 0,1,...,M, \\ j = 0,1,...,N, \end{array} \tag{21b}$$

where $\boldsymbol{F}$ and Q are

$$\boldsymbol{F}(\xi,\eta) = \nabla v(\xi,\eta) - \sum_{s=1}^{4}\boldsymbol{p}^{[s]}(\xi,\eta), \quad Q(\xi,\eta) = \sum_{s=1}^{4} q^{[s]}(\xi,\eta), \tag{22}$$

with $\boldsymbol{p}^{[s]}$ being the penalized boundary conditions enforced along the edges given as

$$\boldsymbol{p}^{[1]}(\xi,\eta) = \sum_{j'=0}^{N} L_{0,j'}(\xi,\eta)\left(\tau^{[1]}\boldsymbol{n}^{[1]}(\mathcal{B}^{[1]}v - g(t))\right)\Big|_{0,j'}, \tag{23a}$$

$$\boldsymbol{p}^{[2]}(\xi,\eta) = \sum_{j'=0}^{N} L_{M,j'}(\xi,\eta)\left(\tau^{[2]}\boldsymbol{n}^{[2]}(\mathcal{B}^{[2]}v - g(t))\right)\Big|_{M,j'}, \tag{23b}$$

$$\boldsymbol{p}^{[3]}(\xi,\eta) = \sum_{i'=0}^{M} L_{i',0}(\xi,\eta)\left(\tau^{[3]}\boldsymbol{n}^{[3]}(\mathcal{B}^{[3]}v - g(t))\right)\Big|_{i',0}, \tag{23c}$$

$$\boldsymbol{p}^{[4]}(\xi,\eta) = \sum_{i'=0}^{M} L_{i',N}(\xi,\eta)\left(\tau^{[4]}\boldsymbol{n}^{[4]}(\mathcal{B}^{[4]}v - g(t))\right)\Big|_{i',N}, \tag{23d}$$

and $q^{[s]}$ being the penalized boundary conditions imposed at the vertices given as

$$\begin{aligned} q^{[1]}(\xi,\eta) =& \frac{L_{0,0}(\xi,\eta)}{\omega_0^\xi}\left(bJ|\nabla\xi|\boldsymbol{n}^{[1]}\cdot\boldsymbol{p}^{[3]}\right)|_{0,0} + \frac{L_{0,N}(\xi,\eta)}{\omega_0^\xi}\left(bJ|\nabla\xi|\boldsymbol{n}^{[1]}\cdot\boldsymbol{p}^{[4]}\right)|_{0,N} \\ &- \frac{L_{0,0}(\xi,\eta)}{\omega_0^\xi}\sigma_{0,0}^{[1]}\left(bJ|\nabla\xi|(\mathcal{B}^{[1]}v - g)\right)|_{0,0} - \frac{L_{0,N}(\xi,\eta)}{\omega_0^\xi}\sigma_{0,N}^{[1]}\left(bJ|\nabla\xi|(\mathcal{B}^{[1]}v - g)\right)|_{0,N}, \end{aligned} \tag{24a}$$

$$
\begin{aligned}
q^{[2]}(\xi,\eta) =& \frac{L_{M,0}(\xi,\eta)}{\omega_M^\xi}\left(bJ|\nabla\xi|\boldsymbol{n}^{[2]}\cdot\boldsymbol{p}^{[3]}\right)|_{M,0} + \frac{L_{M,N}(\xi,\eta)}{\omega_M^\xi}\left(bJ|\nabla\xi|\boldsymbol{n}^{[2]}\cdot\boldsymbol{p}^{[4]}\right)|_{M,N} \\
&- \frac{L_{M,0}(\xi,\eta)}{\omega_M^\xi}\sigma_{M,0}^{[2]}\left(bJ|\nabla\xi|(\mathcal{B}^{[2]}v-g)\right)|_{M,0} - \frac{L_{M,N}(\xi,\eta)}{\omega_M^\xi}\sigma_{M,N}^{[2]}\left(bJ|\nabla\xi|(\mathcal{B}^{[2]}v-g)\right)|_{M,N}, \quad (24b)
\end{aligned}
$$

$$
\begin{aligned}
q^{[3]}(\xi,\eta) =& \frac{L_{0,0}(\xi,\eta)}{\omega_0^\eta}\left(bJ|\nabla\eta|\boldsymbol{n}^{[3]}\cdot\boldsymbol{p}^{[1]}\right)|_{0,0} + \frac{L_{0,N}(\xi,\eta)}{\omega_0^\eta}\left(bJ|\nabla\eta|\boldsymbol{n}^{[3]}\cdot\boldsymbol{p}^{[2]}\right)|_{M,0} \\
&- \frac{L_{0,0}(\xi,\eta)}{\omega_0^\eta}\sigma_{0,0}^{[3]}\left(bJ|\nabla\eta|(\mathcal{B}^{[3]}v-g)\right)|_{0,0} - \frac{L_{0,N}(\xi,\eta)}{\omega_0^\eta}\sigma_{M,0}^{[3]}\left(bJ|\nabla\eta|(\mathcal{B}^{[3]}v-g)\right)|_{M,0}, \quad (24c)
\end{aligned}
$$

$$
\begin{aligned}
q^{[4]}(\xi,\eta) =& \frac{L_{0,N}(\xi,\eta)}{\omega_N^\eta}\left(bJ|\nabla\eta|\boldsymbol{n}^{[4]}\cdot\boldsymbol{p}^{[1]}\right)|_{0,N} + \frac{L_{M,N}(\xi,\eta)}{\omega_N^\eta}\left(bJ|\nabla\eta|\boldsymbol{n}^{[4]}\cdot\boldsymbol{p}^{[2]}\right)|_{M,N} \\
&- \frac{L_{0,N}(\xi,\eta)}{\omega_N^\eta}\sigma_{0,N}^{[4]}\left(bJ|\nabla\eta|(\mathcal{B}^{[4]}v-g)\right)|_{0,N} - \frac{L_{M,N}(\xi,\eta)}{\omega_N^\eta}\sigma_{M,N}^{[4]}\left(bJ|\nabla\eta|(\mathcal{B}^{[4]}v-g)\right)|_{M,N}. \quad (24d)
\end{aligned}
$$

The four edges, $\xi=-1$, $\xi=1$, $\eta=-1$ and $\eta=1$, of a quadrilateral domain are labeled by $s=1,2,3$, and 4, respectively. Variables defined on edge s are then labeled by the superscript $[s]$; for example, $\boldsymbol{n}^{[s]}$ denotes the outward-pointing unit vector function normal to edge s. As shown in Eq. (22), we have two sets of penalty boundary conditions, $\boldsymbol{p}$ and q. Notice that q vanishes at every point except at the four vertices.

We now conduct an energy estimate to determine the values of $\tau^{[s]}$ and $\sigma^{[s]}$. Multiplying $\dot{v}_{i,j}J_{i,j}/a_{i,j}\omega_{i,j}$ to Eq. (21), summing the resultants, applying the quadrature rule dimension by dimension, and doing tedious calculations, we have an energy rate equation

$$
\frac{1}{2}\dot{E} = S^{[1]} + S^{[2]} + S^{[3]} + S^{[4]},
$$

where E is the energy defined as

$$
E = \sum_{i=0}^{M}\sum_{j=0}^{N}\omega_{i,j}\frac{J\dot{v}^2}{a}\Big|_{i,j} + \sum_{i=1}^{M-1}\sum_{j=1}^{N-1}\omega_{i,j}(b\nabla v\cdot\nabla v)\Big|_{i,j}
$$

and $S^{[\nu]}$ for $\nu=1,2,3,4$ are the resulting boundary terms collected according to the edges.

We now show how to determine the values of the penalty parameters on the edge $\xi=-1$ such that the scheme is stable. The explicit form of $S^{[1]}$ is given as

$$
S^{[1]} = \sum_{j=0}^{N}\omega_j^\eta(J|\nabla\xi|)|_{0,j}\dot{\boldsymbol{r}}_j^T\boldsymbol{M}_j\boldsymbol{r}_j,
$$

where $\boldsymbol{r}_j$ are vectors defined as

$$
\boldsymbol{r}_j = \sqrt{b_{0,j}}\left[v_{0,j},\ (\boldsymbol{n}^{[1]}\cdot\nabla v)|_{0,j},\ |\nabla_s v_{0,j}|\right]^T, \quad \nabla_s v = \nabla v - \boldsymbol{n}^{[1]}(\boldsymbol{n}^{[1]}\cdot\nabla v)
$$

and $\boldsymbol{M}_j$ are matrices given as

$$
\boldsymbol{M}_j = \begin{bmatrix} -\alpha(\tau_{0,j}+\delta_{0,j}\sigma_{0,0}+\delta_{N,j}\sigma_{0,N}) & 1-\beta[\tau_{0,j}+\delta_{0,j}\sigma_{0,0}+\delta_{N,j}\sigma_{0,N}] & 0 \\ \alpha\tau|\nabla\xi_{0,j}|^{-1}\omega_0^\xi & -(|\nabla\xi|^{-1}\omega_0^\xi)(1/c_j-\beta\tau) & 0 \\ 0 & 0 & -|\nabla\xi|^{-1}\omega_0^\xi/c_j \end{bmatrix}.
$$

Similar to the one-dimensional analysis, to ensure the stability of the scheme, we need to choose for each j a set of τ and σ such that the upper left 2×2 submatrix of $\boldsymbol{M}_j$ is symmetric semi-negative definite, because $-\omega_0^\xi / c_j < 0$. If we replace the variables $|\nabla \xi|^{-1}$ and ω^ξ in $\boldsymbol{M}_j$ by J and ω, respectively, we observe that for each j the upper left 2×2 submatrix of $\boldsymbol{M}_j$ is identical to the matrix $\boldsymbol{M}$ shown in Eq. (12). Hence, we can make the matrices $\boldsymbol{M}_j$ symmetric semi-negative definite, provided that

$$\tau_{0,j} = \frac{1}{\alpha \omega_0^\xi |\nabla \xi|^{-1} + (1 + \gamma(c_j - 1))\beta}, \quad j = 0, 1, ..., N, \tag{25a}$$

$$\sigma_{0,j} = \gamma(c_j - 1)\tau_{0,j} \quad j = 0, N. \tag{25b}$$

The penalty parameters defined on the rest of the three edges can be obtained with a similar approach. We summarize the results in Table 1.

Table 1: Pointwise values of the penalty parameters. $\gamma \geq 1$. $c_j = 2$ for $j = 0, N$ and $c_j = 1$ otherwise. $c_i = 2$ for $i = 0, M$ and $c_i = 1$ otherwise.

Edge	$1/\tau$		σ	
$\xi = -1$	$\alpha_{0,j}\omega_0^\xi \lvert\nabla\xi\rvert_{0,j}^{-1} + (1+\gamma(c_j-1))\beta_{0,j}$	$j = 0, ..., N$	$\gamma\tau_{0,j}$	$j = 0, N$
$\xi = +1$	$\alpha_{M,j}\omega_M^\xi \lvert\nabla\xi\rvert_{M,j}^{-1} + (1+\gamma(c_j-1))\beta_{M,j}$	$j = 0, ..., N$	$\gamma\tau_{M,j}$	$j = 0, N$
$\eta = -1$	$\alpha_{i,0}\omega_0^\eta \lvert\nabla\eta\rvert_{i,0}^{-1} + (1+\gamma(c_i-1))\beta_{i,0}$	$i = 0, ..., M$	$\gamma\tau_{i,0}$	$i = 0, M$
$\eta = +1$	$\alpha_{i,N}\omega_N^\eta \lvert\nabla\eta\rvert_{i,N}^{-1} + (1+\gamma(c_i-1))\beta_{i,N}$	$i = 0, ..., M$	$\gamma\tau_{i,N}$	$i = 0, M$

2.3.2. Interface boundary condition

We now discuss a way of imposing materials boundary conditions. Without losing generality we consider two attached domains $\Omega^{(1)}$ and $\Omega^{(2)}$ as shown in Fig. 4. Consider $u^{(\nu)}$ for $\nu = 1, 2$ satisfying the IBVP

$$\ddot{u}^{(\nu)}(\boldsymbol{x}, t) = a^{(\nu)} \nabla \cdot \left(b^{(\nu)}(\boldsymbol{x}) \nabla u^{(\nu)}(\boldsymbol{x}, t) \right), \qquad \boldsymbol{x} \in \Omega^{(\nu)}, t > 0, \tag{26a}$$

$$u^{(\nu)}(\boldsymbol{x}, 0) = f^{(\nu)}(\boldsymbol{x}), \quad \dot{u}^{(\nu)}(\boldsymbol{x}, 0) = h^{(\nu)}(\boldsymbol{x}), \qquad \boldsymbol{x} \in \Omega^{(\nu)}, \tag{26b}$$

$$\mathcal{B}^{(\nu)} u^{(\nu)} = \alpha^{(\nu)} u^{(\nu)} + \beta^{(\nu)} \boldsymbol{n} \cdot \nabla u^{(\nu)} = g^{(\nu)}(t), \qquad \boldsymbol{x} \in \partial\Omega_G, t > 0, \tag{26c}$$

$$u^{(1)} = u^{(2)}, \quad \boldsymbol{n}^{(I)} \cdot (b^{(1)} \nabla u^{(1)}) = \boldsymbol{n}^{(I)} \cdot (b^{(2)} \nabla u^{(2)}), \qquad \boldsymbol{x} \in \partial\Omega_I, t > 0, \tag{26d}$$

where $\partial\Omega_G$ is the boundary of the global domain $\bigcup_{\nu=1}^2 \Omega^{(\nu)}$, $\boldsymbol{n}$ is the unit normal vector function on $\partial\Omega_G$, $\partial\Omega_I$ is the interface $\bigcap_{\nu=1}^2 \Omega^{(\nu)}$, and $\boldsymbol{n}$ is the unit normal vector function on $\partial\Omega_I$. For simplicity we assume a homogeneous Neumann boundary condition applied at the global domain boundary. The IBVP has an energy estimate

$$\sum_{\nu=1}^{2} \int_{\Omega^{(\nu)}} \frac{(\dot{u}^{(\nu)})^2}{a^{(\nu)}} + b^{(\nu)} |\nabla u^{(\nu)}|^2 \, d\boldsymbol{x} = \sum_{\nu=1}^{2} \int_{\Omega^{(\nu)}} \frac{(h^{(\nu)})^2}{a^{(\nu)}} + b^{(\nu)} |\nabla f^{(\nu)}|^2 \, d\boldsymbol{x}.$$

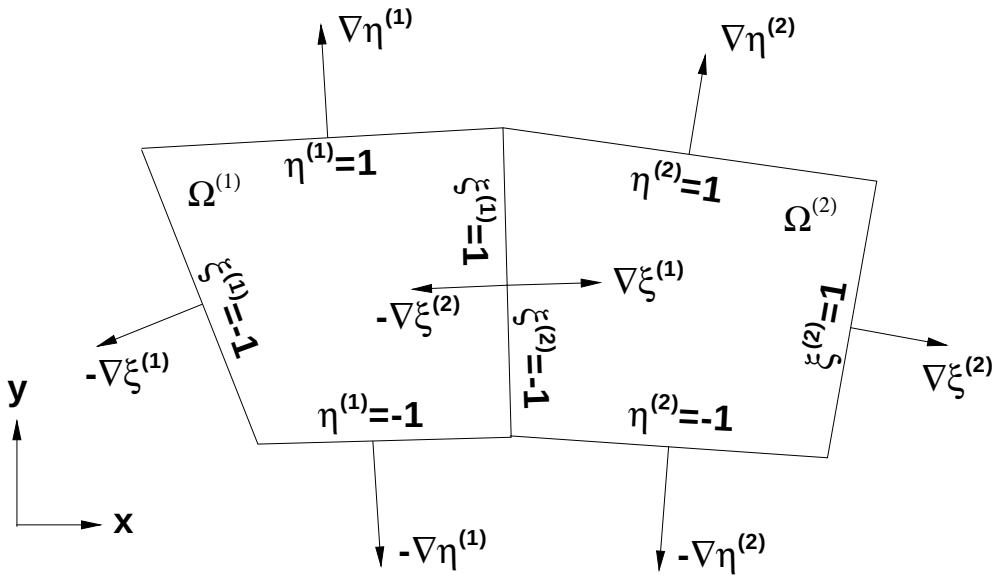

Figure 4: Two attached quadrilateral domains

For each domain we can follow the single domain formulation to construct the scheme shown previously. Here we present the numerical scheme with interface boundary conditions imposed through the penalty methodology. As in the one-dimensional scheme we can define Robin-type boundary operators and the associated boundary conditions along the interface separating two domains. The expressions are

$$\text{on } \Omega^{(1)} \text{ side,} \qquad \mathcal{B}^{(1)}u^{(1)} = u^{(1)} + \beta^{(1)}\boldsymbol{n}^{(1)} \cdot (b^{(1)}\nabla u^{(1)}), \quad g^{(1)} = u^{(2)} + \beta^{(1)}\boldsymbol{n}^{(1)} \cdot (b^{(2)}\nabla u^{(2)}),$$

$$\text{on } \Omega^{(2)} \text{ side,} \qquad \mathcal{B}^{(2)}u^{(2)} = u^{(2)} + \beta^{(2)}\boldsymbol{n}^{(2)} \cdot (b^{(2)}\nabla u^{(2)}), \quad g^{(2)} = u^{(1)} + \beta^{(2)}\boldsymbol{n}^{(2)} \cdot (b^{(1)}\nabla u^{(1)}),$$

where $\boldsymbol{n}^{(1)}$ and $\boldsymbol{n}^{(2)}$ are unit vectors normal to the interface and outward pointing from $\Omega^{(1)}$ and $\Omega^{(2)}$, respectively, and $\beta^{(1)}$ and $\beta^{(2)}$ are positive parameters whose values will be determined later in the stability analysis.

For $\nu = 1, 2$ we seek numerical solutions $v^{(\nu)}$ of the form

$$v^{(\nu)}(\xi^{(\nu)}, \eta^{(\nu)}, t) = \sum_{i=0}^{M^{(\nu)}} \sum_{j=0}^{N} L_{i,j}^{(\nu)}(\xi^{(\nu)}, \eta^{(\nu)}) v_{i,j}^{(\nu)}(t),$$

where $L_{i,j}^{(\nu)}(\xi^{(\nu)}, \eta^{(\nu)})$ are the Lagrange basis polynomials and $v_{i,j}^{(\nu)}(t)$ are field values, defined on $\Omega^{(\nu)}$. We require $v^{(\nu)}$ to satisfy the collocation equations:

$$\frac{J^{(\nu)}\ddot{v}^{(\nu)}}{a^{(\nu)}}\Big|_{i,j} = \frac{\partial\left(b^{(\nu)}J^{(\nu)}\nabla\xi^{(\nu)} \cdot \boldsymbol{F}^{(\nu)}\right)}{\partial\xi^{(\nu)}}\Big|_{i,j} + \frac{\partial\left(b^{(\nu)}J^{(\nu)}\nabla\eta^{(\nu)} \cdot \boldsymbol{F}^{(\nu)}\right)}{\partial\eta^{(\nu)}}\Big|_{i,j} + q_{i,j}^{(\nu)}, \qquad \begin{array}{l} 0 \le i \le M^{(\nu)} \\ 0 \le j \le N \end{array} \tag{27a}$$

$$v_{i,j}^{(\nu)}(0) = f_{i,j}^{(\nu)}, \quad \dot{v}_{i,j}^{(\nu)}(0) = h_{i,j}^{(\nu)}, \qquad 0 \le i \le M^{(\nu)}, \quad 0 \le j \le N, \tag{27b}$$

where

$$\boldsymbol{F}_{i,j}^{(\nu)} = \nabla v_{i,j}^{(\nu)} - \boldsymbol{p}_{i,j}^{(\nu)}, \tag{27c}$$

with $\boldsymbol{p}_{i,j}^{(\nu)}$ and $q_{i,j}^{(\nu)}$ being the pointwise values of the penalized interface boundary conditions. The explicit forms of $\boldsymbol{p}^{(\nu)}(\xi,\eta)$ and $q^{(\nu)}(\xi,\eta)$ are given as

$$\boldsymbol{p}^{(1)}(\xi^{(1)},\eta^{(1)}) = \sum_{j'=0}^{N} L_{M^{(1)},j'}^{(1)}\left(\xi^{(1)},\eta^{(1)}\right)\tau_{M^{(1)},j'}^{(1)}\boldsymbol{n}_{M^{(1)},j'}^{(1)}\delta v_{M^{(1)},j'}^{(1)}$$

$$\boldsymbol{p}^{(2)}(\xi^{(2)},\eta^{(2)}) = \sum_{j'=0}^{N} L_{0,j'}^{(2)}\left(\xi^{(2)},\eta^{(2)}\right)\tau_{0,j'}^{(2)}\boldsymbol{n}_{0,j'}^{(2)}\delta v_{0,j'}^{(2)}$$

$$\begin{aligned}
q^{(1)}(\xi^{(1)},\eta^{(1)}) = &-\frac{L_{M^{(1)},0}^{(1)}(\xi^{(1)},\eta^{(1)})}{\omega_{M^{(1)}}^{\xi}}\sigma_{M^{(1)},0}^{(1)}\left(b^{(1)}J^{(1)}|\nabla\xi^{(1)}|(\delta v^{(1)})\right)|_{M^{(1)},0} \\
&-\frac{L_{M^{(1)},N}^{(1)}(\xi^{(1)},\eta^{(1)})}{\omega_{M^{(1)}}^{\xi}}\sigma_{M^{(1)},N}^{(1)}\left(b^{(1)}J^{(1)}|\nabla\xi^{(1)}|(\delta v^{(1)})\right)|_{M^{(1)},N}, \\
q^{(2)}(\xi^{(2)},\eta^{(2)}) = &-\frac{L_{0,0}^{(2)}(\xi^{(2)},\eta^{(2)})}{\omega_{0}^{\xi}}\sigma_{0,0}^{(2)}\left(b^{(2)}J^{(2)}|\nabla\xi^{(2)}|(\delta v^{(2)})\right)|_{0,0} \\
&-\frac{L_{0,N}^{(2)}(\xi^{(2)},\eta^{(2)})}{\omega_{0}^{\xi}}\sigma_{0,N}^{(2)}\left(b^{(2)}J^{(2)}|\nabla\xi^{(2)}|(\delta v^{(2)})\right)|_{0,N}
\end{aligned}$$

with

$$\begin{aligned}
\delta v_{M^{(1)},j'}^{(1)} &= \left[(v_{M^{(1)},j'}^{(1)} - v_{0,j'}^{(2)}) + (\beta^{(1)}\boldsymbol{n}^{(1)})|_{M^{(1)},j'}\cdot((b^{(1)}\nabla v^{(1)})|_{M^{(1)},j'} - (b^{(2)}\nabla v^{(2)})|_{0,j'})\right] \\
\delta v_{0,j'}^{(2)} &= \left[(v_{0,j'}^{(2)} - v_{M^{(1)},j'}^{(1)}) + (\beta^{(2)}\boldsymbol{n}^{(2)})|_{0,j'}\cdot((b^{(2)}\nabla v^{(2)})|_{0,j'} - (b^{(1)}\nabla v^{(1)}|_{M^{(1)},j'})\right].
\end{aligned}$$

We now conduct an energy estimate to determine the pointwise values of $\beta^{(\nu)}$, $\tau^{(\nu)}$, and $\sigma^{(\nu)}$ on the interface. Multiplying $(J^{(\nu)}\dot{v}^{(\nu)}\omega^{(\nu)})|_{i,j}$ to Eqs. (27), summing the resultants, invoking the quadrature rule of integration, and doing tedious calculations, we obtain an energy estimate

$$\dot{E} = \sum_{j=0}^{N}\omega_j^E J^E 2\dot{\boldsymbol{r}}_j^T\boldsymbol{M}_j\boldsymbol{r}_j,$$

where E is the energy given as

$$E = \sum_{\nu=1}^{2}\left(\sum_{i=0}^{M^{(\nu)}}\sum_{j=0}^{N_\eta}\omega_{i,j}^{(\nu)}\frac{J^{(\nu)}(\dot{v}^{(\nu)})^2}{a^{(\nu)}}\Big|_{i,j} + \sum_{i=1}^{M^{(\nu)}-1}\sum_{j=1}^{N-1}\omega_{i,j}^{(\nu)}(b^{(\nu)}\nabla v^{(\nu)}\cdot\nabla v^{(\nu)})\Big|_{i,j}\right).$$

Here, $\omega_j^E = \omega_j^\eta$, $J_j^E = (J^{(1)}|\nabla\xi^{(1)}|)|_{M^{(1)},j} = (J^{(2)}|\nabla\xi^{(2)}|)|_{0,j}$, $\boldsymbol{r}_j$ are vectors defined as

$$\boldsymbol{r}_j = \left[v_{M^{(1)},j}^{(1)},\, v_{0,j}^{(2)},\, \left(b^{(1)}\frac{\partial v^{(1)}}{\partial n}\right)\Big|_{M^{(1)},j},\, -\left(b^{(2)}\frac{\partial v^{(2)}}{\partial n}\right)\Big|_{0,j},\, \left(b^{(1)}|\nabla_s v^{(1)}|\right)\Big|_{M^{(1)},j},\, \left(b^{(2)}|\nabla_s v^{(2)}|\right)\Big|_{0,j}\right]^T,$$

and $\boldsymbol{M}_j$ are 6×6 matrices of the form

$$\boldsymbol{M}_j = \begin{bmatrix} \boldsymbol{M}_U & \mathbf{0} \\ \mathbf{0}^T & \boldsymbol{M}_L \end{bmatrix}$$

with $\mathbf{0}$ denoting the 4×2 zero matrix, $\boldsymbol{M}_L = \text{diag}\left(-\bar{\omega}^{(1)}_{M^{(1)},j}/(b^{(1)}c_j), -\bar{\omega}^{(2)}_{0,j}/(b^{(2)}c_j)\right)$, and

$$\boldsymbol{M}_U = \begin{bmatrix} -\widetilde{\tau}^{(1)}b^{(1)}|_{M^{(1)},j} & \widetilde{\tau}^{(1)}b^{(1)}|_{M^{(1)},j} & 1-\widetilde{\tau}^{(1)}\beta^{(1)}b^{(1)}|_{M^{(1)},j} & \widetilde{\tau}^{(1)}\beta^{(1)}b^{(1)}|_{M^{(1)},j} \\ \widetilde{\tau}^{(2)}b^{(2)}|_{0,j} & -\widetilde{\tau}^{(2)}b^{(2)}|_{0,j} & -\widetilde{\tau}^{(2)}\beta^{(2)}b^{(2)}|_{0,j} & -(1-\widetilde{\tau}^{(2)}\beta^{(2)}b^{(2)}|_{0,j}) \\ \tau^{(1)}\bar{\omega}^{(1)}|_{M^{(1)},j} & -\tau^{(1)}\bar{\omega}^{(1)}|_{M^{(1)},j} & -(1/(cb^{(1)})-\tau^{(1)}\beta^{(1)})\bar{\omega}^{(1)}|_{M^{(1)},j} & -\tau^{(1)}\bar{\omega}^{(1)}\beta^{(1)}|_{M^{(1)},j} \\ \tau^{(2)}\bar{\omega}^{(2)}|_{0,j} & -\tau^{(2)}\bar{\omega}^{(2)}|_{0,j} & -\tau^{(2)}\beta^{(2)}\bar{\omega}^{(2)}|_{0,j} & -(1/(cb^{(2)})-\tau^{(2)}\beta^{(2)})\bar{\omega}^{(2)}|_{0,j} \end{bmatrix},$$

$$\widetilde{\tau}^{(\nu)} = \tau^{(\nu)} + \sigma^{(\nu)}, \quad \bar{\omega}^{(1)}_{M^{(1)},j} = \frac{2}{M^{(1)}(M^{(1)}+1)|\nabla\xi^{(1)}|_{M^{(1)},j}}, \quad \bar{\omega}^{(2)}_{0,j} = \frac{2}{M^{(2)}(M^{(2)}+1)|\nabla\xi^{(2)}|_{0,j}}.$$

For stability we need to choose the values of $\tau^{(\nu)}$, $\sigma^{(\nu)}$, and $\beta^{(\nu)}$ such that for each j the matrix $\boldsymbol{M}_j$ is symmetric semi-negative definite. Since $\boldsymbol{M}_L$ is diagonal and negative definite, it is sufficient to choose the parameters such that $\boldsymbol{M}_U$ is symmetric semi-negative definite. Notice that for each j, $\boldsymbol{M}_U$ and the matrix $\boldsymbol{M}$ in Eq. (19) are of the same form. Hence, to make $\boldsymbol{M}_U$ symmetric semi-negative definite, we take

$$\beta^{(1)}_{M^{(1)},j} = \frac{\bar{\omega}^{(2)}}{(1+\gamma(c-1))b^{(2)}}\Big|_{M^{(1)},j}, \quad \tau^{(1)}_{M^{(1)},j} = \frac{b^{(2)}}{b^{(2)}\bar{\omega}^{(1)}+b^{(1)}\bar{\omega}^{(2)}}\Big|_{M^{(1)},j}, \quad \sigma^{(1)}_{M^{(1)},j} = \gamma(c-1)\tau^{(1)}_{M^{(1)},j}, \tag{28a}$$

$$\beta^{(2)}_{0,j} = \frac{\bar{\omega}^{(1)}}{(1+\gamma(c-1))b^{(1)}}\Big|_{0,j}, \quad \tau^{(2)}_{0,j} = \frac{b^{(1)}}{b^{(2)}\bar{\omega}^{(1)}+b^{(1)}\bar{\omega}^{(2)}}\Big|_{0,j}, \quad \sigma^{(2)}_{0,j} = \gamma(c-1)\tau^{(2)}\Big|_{0,j} \tag{28b}$$

with $\gamma \geq 1$.

In the above formulation the edges on the two quadrilaterals are described by the equations $\xi^{(\nu)} = \pm 1$ and $\eta^{(\nu)} = \pm 1$ for $\nu = 1, 2$, and the interface is described by $\xi^{(1)} = 1$ and $\xi^{(2)} = -1$. We have shown how to determine the values of the associated parameters τ, σ, and β at the interface grid points such that the scheme is stable. For an interface described by other edges of the two domains, one can follow a similar approach to determine the values of the associated parameters needed to ensure stable computations.

2.4. Time integration

To march numerical solutions in time, we adopt the RKN method [34] which is fourth-order accurate. Denote the time step by Δt and the nth time level by $t^n = n\Delta t$. Let v^n be the numerical solution at time t^n. The RKN method for a second-order differential equation of the form $\ddot{v} = \mathcal{F}(t, v, \dot{v})$ involves the following steps:

Intermediate steps:

$$K_1 = \mathcal{F}\left(t^n,\, v^n,\, \dot{v}^n\right), \tag{29a}$$

$$K_2 = \mathcal{F}\left(t^n + \frac{\Delta t}{2},\, v^n + \frac{\Delta t}{2}\dot{v}^n + \frac{(\Delta t)^2}{8}K_1,\, \dot{v}^n + \frac{\Delta t}{2}K_1\right), \tag{29b}$$

$$K_3 = \mathcal{F}\left(t^n + \frac{\Delta t}{2}, v^n + \frac{\Delta t}{2}\dot{v}^n + \frac{(\Delta t)^2}{8}K_1,\, \dot{v}^n + \frac{\Delta t}{2}K_2\right), \tag{29c}$$

$$K_4 = \mathcal{F}\left(t^n + \Delta t,\, v^n + \Delta t\dot{v}^n + \frac{(\Delta t)^2}{2}K_3,\, \dot{v}^n + \Delta t K_3\right), \tag{29d}$$

Update step:

$$v^{n+1} = v^n + \Delta t\left(\dot{v}^n + \frac{\Delta t}{6}(K_1 + K_2 + K_3)\right), \quad \dot{v}^{n+1} = \dot{v}^n + \frac{\Delta t}{6}(K_1 + 2K_2 + 2K_3 + K_4). \tag{29e}$$

Notice that the wave equation considered in the present study does not involve $\dot{v}$. Thus, we have $K_3 = K_2$ in the RKN method to simplify computations.

If the imposed boundary condition $g(t)$ is an explicit time-dependent function, then special treatments are needed to avoid order reduction of the RKN method. The reason is that the explicit time function introduced to the scheme leads to an inaccurate approximation at the final update step. To recover the correct convergence rate of the present method, we follow a similar analysis shown in [5] and obtain approximations of $g(t)$ at the intermediate time levels $t^n + \Delta t/2$ and $t^n + \Delta t$ by $g(t^n)$ and the derivatives of $g(t^n)$ as

$$g\left(t^n + \frac{\Delta t}{2}\right) \approx g(t_n) + \frac{\Delta t}{2}g'(t_n) + \frac{(\Delta t)^2}{8}g''(t_n), \tag{30a}$$

$$g\left(t^n + \Delta t\right) \approx g(t_n) + \Delta t g'(t_n) + \frac{(\Delta t)^2}{2}g''(t_n) + \frac{(\Delta t)^3}{4}g'''(t_n) + \frac{(\Delta t)^4}{16}g''''(t_n), \tag{30b}$$

where $'$ denotes the differentiation with respect to the time variable t.

A formula for adaptively computing the time step, which has taken the grid distortion into account, was given in [20] for multidomain pseudospectral wave simulations. For the present study we modify the formula and compute the time step Δt as follows:

$$\Delta t = \mathrm{CFL} \times \min_{\boldsymbol{x}\in\Omega}\left(\sqrt{a(\boldsymbol{x})b(\boldsymbol{x})}|\boldsymbol{\chi}|\right)^{-1}, \quad \boldsymbol{\chi} = |\nabla\xi|/\Delta\xi_i + |\nabla\eta|/\Delta\eta_j,$$

where CFL is designated as the Courant-Friedrichs-Lewy number, $(a(\boldsymbol{x})b(\boldsymbol{x}))^{1/2}$ is the local wave speed, $\boldsymbol{\chi}$ is the local grid distortion vector, $\Delta\xi_i$ and $\Delta\eta_j$ represent the local grid sizes, and $|\nabla\xi|$ and $|\nabla\eta|$ in this particular notation are given by

$$|\nabla\xi| = \left(\left|\frac{\partial\xi}{\partial x}\right|, \left|\frac{\partial\xi}{\partial y}\right|\right), \quad |\nabla\eta| = \left(\left|\frac{\partial\eta}{\partial x}\right|, \left|\frac{\partial\eta}{\partial y}\right|\right).$$

In this study we use CFL ≤ 0.6 for stable computations after a series of numerical tests.

3. Numerical Results

3.1. Error and convergence rate

We have conducted a series of numerical experiments based on the present methods. For each computation we measure the maximum error defined as $e(N) = ||u - u_N||_\infty$, where u is the exact solution and u_N is the numerical solution corresponding to polynomial degree N. The convergence order denoted by q is calculated as

$$q = \frac{1}{2}\frac{\log(e(N_1)/e(N_2))}{\log(N_2/N_1)},$$

where the extra factor 1/2 results from the minimum grid point size, which scales like $1/N^2$. In this section we provide one- and two-dimensional computational results of the experiments.

Example 1. *Let* $\mathsf{I} = [-1, 1]$. *Consider* $u(x,t) = \sin(1.5\pi(x-t))$ *satisfying following the problem:*

$$\begin{aligned}
\ddot{u}(x,t) &= u''(x,t), && x \in \mathsf{I}, \quad t > 0,\\
u(x,0) &= \sin(1.5\pi x), \quad \dot{u}(x,0) = -1.5\pi\cos(1.5\pi x), && x \in \mathsf{I},\\
\mathcal{B}_L u(-1,t) &= \alpha_L \sin(1.5\pi(-1-t)) - \beta_L(1.5\pi)\cos(1.5\pi(-1-t)), && t > 0,\\
\mathcal{B}_R u(+1,t) &= \alpha_R \sin(1.5\pi(+1-t)) + \beta_R(1.5\pi)\cos(1.5\pi(+1-t)), && t > 0.
\end{aligned}$$

Our first experiment examines the convergence property of the scheme with boundary conditions imposed at the RKN intermediate stage. We numerically solve the problem with and without applying Eqs. (30a)–(30b) at the intermediate stages. Results of the convergence study are presented in Table 2. We observe order reduction of the RKN method if the scheme is without correction at the intermediate stages. If the modification is made at the intermediate stages, then the correct convergence order is recovered.

Table 2: Convergence study results of the scheme with and without correction at the RKN intermediate stages for Example 1. T=1.25. $\alpha_L = 1$, $\beta_L = 0$, $\alpha_R = 1$, $\beta_R = 0$

N	Without Modification		With Modification	
	$e(N)$	q	$e(N)$	q
12	2.0285e-03	-	1.7045e-03	-
16	9.4277e-05	5.33	2.5561e-06	11.3
20	4.1925e-05	1.81	3.7849e-07	4.27
24	1.9125e-05	2.15	8.8487e-08	3.98
28	1.0223e-05	2.03	2.5880e-08	3.98

Tables 3–5 present convergence study results of the method solving the problem subject to different types of boundary conditions applied at $x = \pm 1$. It is shown that for each terminal time T the error decays as N

increases and the convergence rate is of fourth order. Moreover, we observe that for a fixed grid resolution N the error increases approximately linearly in time, indicating that the scheme is also time stable.

Table 3: Convergence study for Example 1 at different terminal times. $\alpha_L = 1$, $\beta_L = 0$, $\alpha_R = 1$, $\beta_R = 0$.

N	$T = 1$		$T = 10$		$T = 100$	
	$e(N)$	q	$e(N)$	q	$e(N)$	q
12	1.4470e-03	-	1.1860e-02	-	1.1752e-01	-
16	1.1732e-05	8.36	1.8494e-04	7.23	1.6699e-03	7.39
20	1.9744e-06	3.99	3.1507e-05	3.96	2.7914e-04	4.00
24	4.6719e-07	3.95	7.3324e-06	3.99	6.5020e-05	3.99

Table 4: Convergence study for Example 1 at different terminal times. $\alpha_L = 1$, $\beta_L = 0$, $\alpha_R = 0$, $\beta_R = 1$.

N	$T = 1$		$T = 10$		$T = 100$	
	$e(N)$	q	$e(N)$	q	$e(N)$	q
12	1.4363e-03	-	1.1808e-02	-	1.1736e-01	-
16	3.6827e-05	6.36	1.1135e-05	12.1	1.0532e-04	12.2
20	6.1740e-06	4.00	8.9822e-07	5.64	9.4168e-06	5.41
24	1.4398e-06	3.99	2.3073e-07	3.72	2.1910e-06	3.99

Table 5: Convergence study for Example 1 at different terminal times. $\alpha_L = 1$, $\beta_L = 0$, $\alpha_R = 1$, $\beta_R = 0.5$

N	$T = 1$		$T = 10$		$T = 100$	
	$e(N)$	q	$e(N)$	q	$e(N)$	q
12	1.4349e-03	-	1.1819e-02	-	1.1742e-01	-
16	2.7994e-05	6.84	4.6733e-05	9.61	1.0524e-04	12.2
20	4.6969e-06	3.99	7.5846e-06	4.07	3.0923e-06	7.90
24	1.0848e-06	4.01	1.7765e-06	3.98	7.4317e-07	3.91

3.2. hp-convergence

Example 2. *Let* $\Omega = [-1,1]^2$. *Consider* $u = \sin(\pi(x+y-\sqrt{2}t))$ *satisfying the IBVP:*

$$\begin{aligned}
\ddot{u}(x,y,t) &= \nabla^2 u(x,y,t), && (x,y) \in \Omega, t \geq 0 \\
u(x,y,0) &= \sin(\pi(x+y)), \quad \dot{u}(x,y,0) = -\sqrt{2}\pi\cos(\pi(x+y)), && (x,y) \in \Omega, \\
u(\pm 1,y,t) &= \sin(\pi(\pm 1 + y - \sqrt{2}t), && y \in [-1,1], t > 0 \\
u(x,\pm 1,t) &= \sin(\pi(x \pm 1 - \sqrt{2}t), && x \in [-1,1], t > 0.
\end{aligned}$$

We use structural and unstructured multidomain meshes (see Figs. 5(a)–5(d)) to simulate wave propagations. For a given mesh the grid resolutions N and M within each element are set equal. A Dirichlet boundary condition is assigned on a subdomain edge if it is a piece of the global domain boundary. To patch field values between elements, we assign continuous interface conditions at these domain edges.

Convergence study results are given in Table 6. For the computations based on a structural mesh we observe p-convergence as the grid resolution N increases, and the convergence rate is of fourth order. While the total number of domains increases for a constant N, we see h-convergence. For the computations based on the unstructured mesh we observe exponential convergence. This rapid convergence is due to the fact that distorted subdomains lead to a smaller time step and the error is dominated by the spatial approximation. Wave field profiles computed by the present methods are shown in Fig. 6.

Table 6: Convergence study results for Example 2 at $T = 10$. The computational meshes are shown in Fig. 5(a-d). $\gamma = 1$ for computations based on structural meshes and $\gamma = 1.2$ for computations based on the unstructured mesh.

N	1 Domain		4 Domains		16 Domains		9 Domains	
	$e(N)$	q	$e(N)$	q	$e(N)$	q	$e(N)$	q
8	3.2601e-03	-	3.2713e-05	-	8.2056e-07	-	3.5017e-04	-
12	9.3474e-06	7.21	5.1471e-07	5.12	3.2102e-08	3.99	5.8834e-08	10.71
16	8.8419e-07	4.09	5.6301e-08	3.84	3.5116e-09	3.84	7.1608e-10	7.66
20	1.5723e-07	3.86	9.9412e-09	3.88	6.1744e-10	3.89	1.3077e-10	3.81

Here we address an issue related to the penalty strength parameter γ. In this example we use $\gamma = 1$ for computations based on the structural meshes, and we use $\gamma = 1.2$ for computations based on the unstructured mesh because of numerical instability. In Fig. 7 we present the error histories for the computations based on the unstructured mesh with different values of γ. The results show that the computations are unstable for $\gamma = 1.0$ and $\gamma = 1.1$ and that the computation becomes stable for $\gamma = 1.2$. These results are consistent with the theoretical analysis since increasing the value of γ increases the dissipation in the scheme. Although the penalty strength parameter plays a role in suppressing the instability, we note that the stability condition $\gamma \geq$

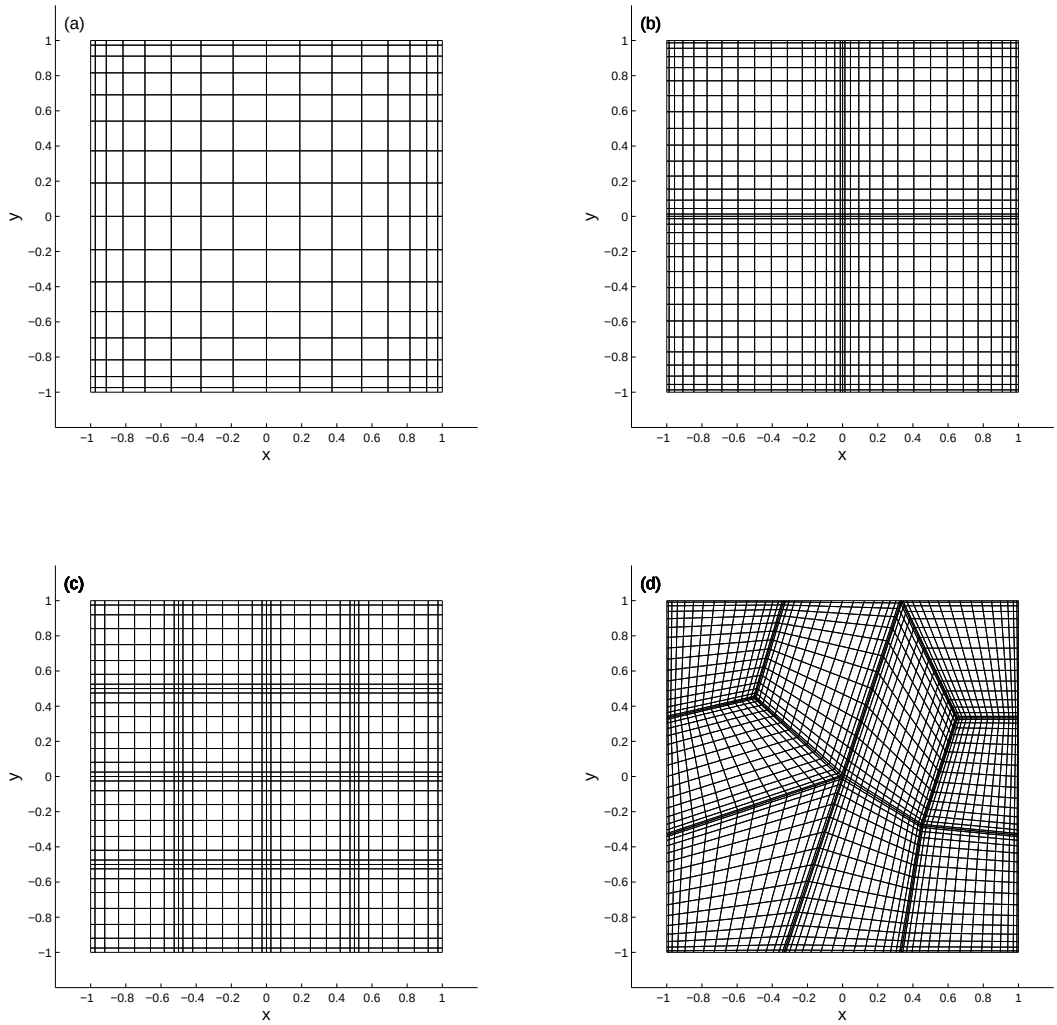

Figure 5: Structural meshes composed of 1 domain (a), 4 subdomains (b), and 16 subdomains (c). Unstructured mesh composed of 9 subdomains (d).

1 obtained from the analysis shown in Section 2 is only a necessary condition but not sufficient. Hence, the numerical instabilities due to severe grid distortions may not be eliminated completely by simply increasing the value of γ. In this situation a possible way to suppress the instability is to introduce more dissipation to the scheme through filtering. This approach has been widely used in pseudospectral computations for partial differential equations. Since the filtering issue is beyond the scope of this study, we refer the reader to [23] for further details.

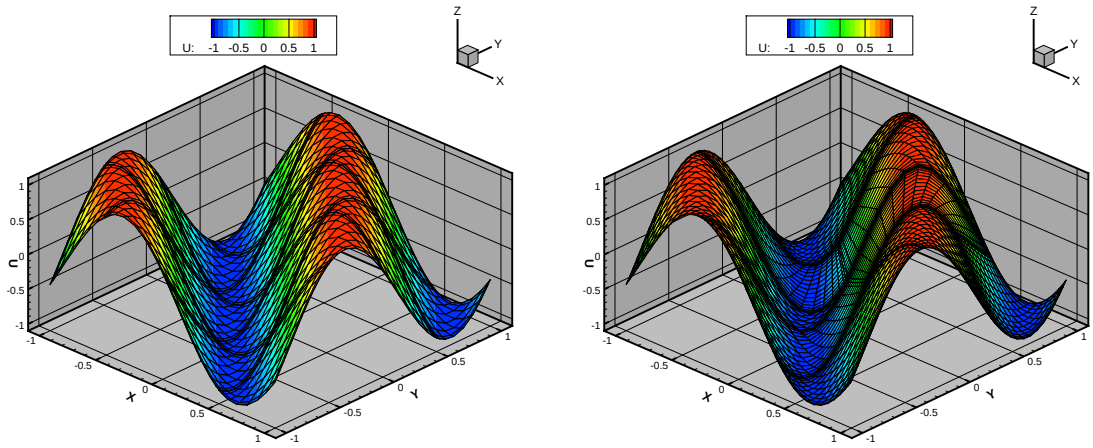

Figure 6: Wave fields computed by the present method for Example 2 based on the 16-domain structural mesh (see Fig. 5(c)) and the unstructured 9-domain mesh (see Fig. 5(d)).

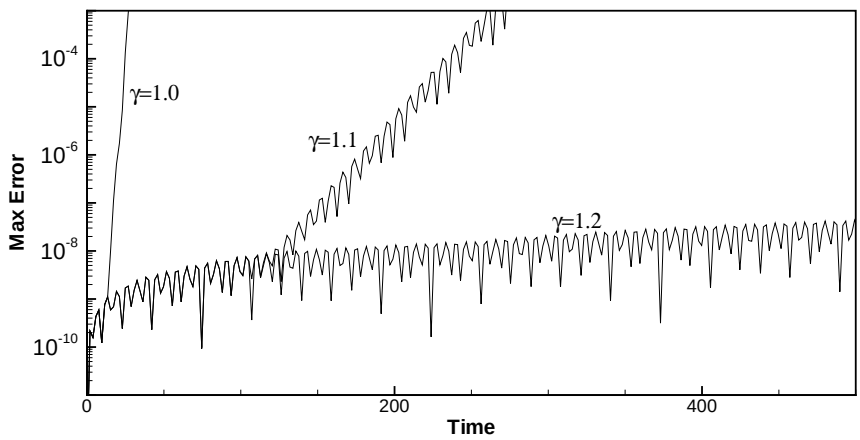

Figure 7: Error history for Example 2 based on the unstructured mesh shown in Fig. 6 with grid resolutions $M = N = 16$, for $\gamma = 1.0$, $1, 1$ and 1.2.

3.3. Problem involving material discontinuity

Example 3. *Let* $\Omega^{(1)} = [-1, 0] \times [-1, 1]$, $\Omega^{(2)} = [0, 1] \times [-1, 1]$ *and* $\Omega = [-1, 1]^2$. *We consider the following problem:*

$$\ddot{u}^{(1)}(x, y, t) = \frac{1}{2}\nabla^2 u^{(1)}(x, y, t), \qquad (x, y) \in \Omega^{(1)},\ t > 0$$

$$\ddot{u}^{(2)}(x, y, t) = \frac{1}{5}\nabla^2 u^{(2)}(x, y, t), \qquad (x, y) \in \Omega^{(2)},\ t > 0$$

$$u^{(1)}(x, y, 0) = \sin(\pi x)\sin(\pi y), \quad \dot{u}^{(1)}(x, y, 0) = 0, \qquad (x, y) \in \Omega^{(1)},$$

$$u^{(2)}(x, y, 0) = \sqrt{\frac{5}{8}}\sin(2\pi x)\sin(\pi y), \quad \dot{u}^{(2)}(x, y, 0) = 0, \qquad (x, y) \in \Omega^{(2)},$$

$$u^{(1)}(x,y,t) = u^{(2)}(x,y,t) = 0, \qquad (x,y) \in \partial\Omega,\ t > 0$$

$$u^{(1)}(0,y,t) = u^{(2)}(0,y,t), \quad \frac{1}{\sqrt{2}}\frac{\partial u^{(1)}(0,y,t)}{\partial x} = \frac{1}{\sqrt{5}}\frac{\partial u^{(2)}(0,y,t)}{\partial x}, \qquad y \in [-1,1],\ t > 0,$$

where $\partial\Omega$ denotes the domain boundary of the global domain Ω.

The analytic forms of $u^{(1)}$ and $u^{(2)}$ are

$$u^{(1)}(x,y,t) = \sin(\pi x)\sin(\pi y)\cos(\pi t), \quad u^{(2)}(x,y,t) = \sqrt{\frac{5}{8}}\sin(2\pi x)\sin(\pi y)\cos(\pi t).$$

To solve the problem, we decompose the domain $[-1,1]^2$ into four equal-sized squares as shown in Fig. 5(b). At adjacent subdomain edges we enforce continuous interface boundary conditions for patching field values.

Table 7 presents results of a grid convergence study. For each terminal time T ($T = 1, 10, 100$) we see that as N increases, the error rapidly decays and the convergence rate gradually recovers a fourth order. This numerical experiment shows that the penalized interface boundary conditions do effectively patch the field values in between subdomains even for discontinuous material coefficients at interfaces. For completeness we illustrate the computed field plot at $T = 1$ in Fig. 8.

Table 7: Convergence study results for Example 3 at different terminal times.

N	$T = 1$		$T = 10$		$T = 100$	
	$e(N)$	q	$e(N)$	q	$e(N)$	q
8	9.4735e-04		1.6679e-03		1.5173e-03	
10	3.9624e-05	7.11	3.4855e-05	8.66	4.4049e-05	7.93
12	4.4145e-07	12.33	5.7483e-07	11.25	3.2956e-07	13.42
14	7.3508e-09	13.22	7.3004e-09	14.16	2.0455e-08	9.01
16	6.1655e-11	17.99	5.6466e-10	9.58	5.6832e-09	4.79

3.4. Curvilinear domain problems

The preceding examples were based on meshes composed of straight-sided domains. We now provide convergence studies of our method for simulating waves involving curvilinear domains.

3.4.1. Waves in a circular disk

Example 4. *Let $\Omega = \{(r,\theta)|0 \le r \le 2,\ 0 \le \theta \le 2\pi\}$, and consider $u(r,\theta,t)$ satisfying the following problem:*

$$\ddot{u}(r,\theta,t) = \nabla^2 u(r,\theta,t), \qquad (r,\theta) \in \Omega,\ t > 0,$$

$$u(r,\theta,0) = J_3(k_r r)\cos(3\theta), \quad \dot{u}(r,\theta,0) = k_r J_3(k_r r)\sin(3\theta), \qquad (r,\theta) \in \Omega,$$

$$u(2,\theta,t) = 0, \qquad 0 \le \theta \le 2\pi,\ t > 0,$$

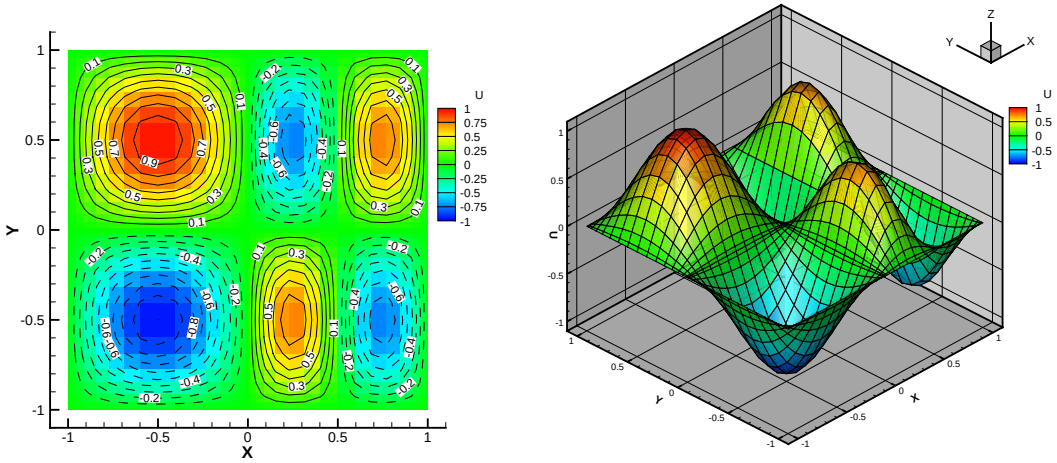

Figure 8: Color contour (left) 3D field (right) plots of the simulated wave fields, $u^{(1)}$ and $u^{(2)}$ in Example 3, at $T = 1$.

where J_3 is the third-order Bessel function of the first kind.

The exact solution to the problem is given as

$$u(r, \theta, t) = J_3(k_r r)\cos(3\theta - k_r t), \quad k_r = 3.190080947961992.$$

A mesh composed of twelve domains as shown in Fig. 9, with some subdomains being curvilinear, is used for computations. The convergence study results are given in Table 8. We observe that for each terminal time the error vanishes rapidly as the degree of the approximation polynomial increases.

In this example we use $\gamma = 1.2$ for computations because of numerical instability. In Fig. 10 we present the error histories for the computations with different values of γ. The results show that the computations are unstable for $\gamma = 1.0$ and $\gamma = 1.1$ and that the computation becomes stable for $\gamma = 1.2$.

Table 8: Convergence study results for Example 4. The terminal time T is expressed in terms of the fundamental period in time $p = 1.9696000586842051$.

N	$T = 1p$		$T = 10p$		$T = 100p$	
	$e(N)$	q	$e(N)$	q	$e(N)$	q
8	6.6186e-05	-	2.7843e-04	-	4.6362e-04	-
10	1.5325e-06	8.43	2.6015e-06	10.47	7.3705e-06	9.28
12	2.5946e-08	11.18	1.5916e-08	13.97	1.0749e-07	11.59
14	4.2829e-10	13.31	1.0327e-09	8.87	1.0168e-08	7.64
16	3.5059e-11	9.37	3.4481e-10	4.10	3.4526e-09	4.04

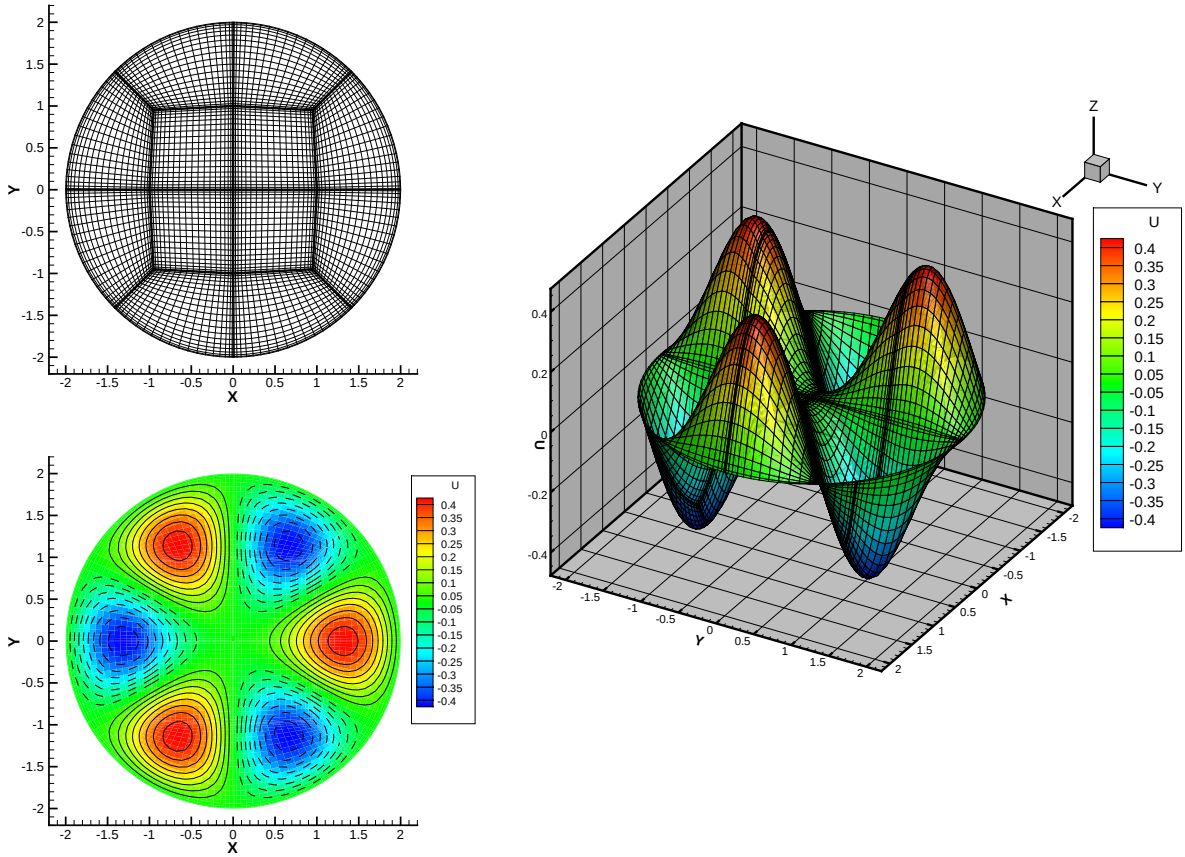

Figure 9: Multidomain mesh for waves in a circular domain (top left), contour field plot of a wave (bottom left), and 3D field plot of a wave in the circular domain (right).

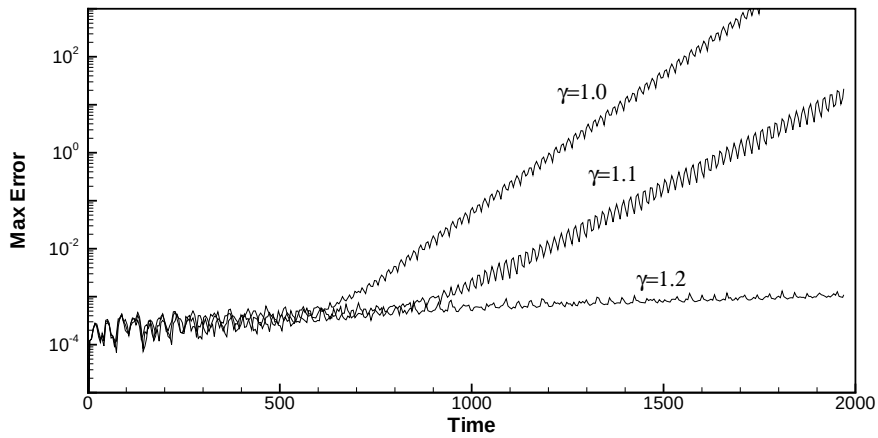

Figure 10: Error history for Example 4 based on the mesh shown in Fig. 9 with grid resolutions $M = N = 8$.

3.4.2. Waves in a ring waveguide

Our fifth experiment involves simulating a wave in a ring waveguide.

Example 5. *Consider the regions* $\Omega^{(1)} = \{(r,\theta)|2 \le r \le 2.5,\, 0 \le \theta \le 2\pi\}$ *and* $\Omega^{(2)} = \{(r,\theta)|2.5 \le r \le 3.0,\, 0 \le \theta \le 2\pi\}$. *Within* $\Omega^{(1)}$ *the coefficients are* $a^{(1)} = b^{(1)} = 0.5$, *and within* $\Omega^{(2)}$ *the coefficients are* $a^{(2)} = b^{(2)} = 5$. *We consider wave functions* $u^{(\nu)}(r,\theta,t)$ *for* $\nu = 1,2$ *satisfying the IBVP:*

$$
\begin{aligned}
&\ddot{u}^{(\nu)} = a^{(\nu)}\nabla\cdot(b^{(\nu)}\nabla u^{(\nu)}), && (r,\theta)\in\Omega^{(\nu)}, t>0,\\
&u^{(\nu)} = (A^{(\nu)}J_8(k^{(\nu)}r) + B^{(\nu)}Y_8(k^{(\nu)}r))\cos(8\theta), && (r,\theta)\in\Omega^{(\nu)}, t=0,\\
&\dot{u}^{(\nu)} = k^{(\nu)}\sqrt{a^{(\nu)}b^{(\nu)}}(A^{(\nu)}J_8(k^{(\nu)}r) + B^{(\nu)}Y_8(k^{(\nu)}r))\sin(8\theta) && (r,\theta)\in\Omega^{(\nu)}, t=0,\\
&u^{(1)}(2,\theta,t) = u^{(2)}(3,\theta,t) = 0, && \theta\in(0,2\pi), t>0,\\
&u^{(1)}(2.5,\theta,t) = u^{(2)}(2.5,\theta,t), && \theta\in(0,2\pi), t>0,\\
&\boldsymbol{n}\cdot(b^{(1)}\nabla u^{(1)}(2.5,\theta,t) - b^{(2)}\nabla u^{(2)}(2.5,\theta,t)) = 0, && \theta\in(0,2\pi), t>0,
\end{aligned}
$$

where J_8 *and* Y_8 *are the eighth-order Bessel functions of the first and the second kinds, respectively.*

The solutions $u^{(\nu)}$ for $\nu = 1,2$ are given as

$$
u^{(\nu)} = \left(A^{(\nu)}J_8(k^{(\nu)}r) + B^{(\nu)}Y_8(k^{(\nu)}r)\right)\cos\left(8\theta - k^{(\nu)}\sqrt{a^{(\nu)}b^{(\nu)}}t\right) \tag{31}
$$

with parameters provided in Table 9.

Table 9: Parameters used is Eq. (31)

ν	$k^{(\nu)}$	$A^{(\nu)}$	$B^{(\nu)}$
1	6.91653857590121	-0.000933627891442	-0.003076893577698
2	0.69165385759012	-0.999994830519074	-0.000000021132401

We use a computational mesh composed of sixteen domains as shown in Fig. 11. The results of the convergence study are provided in Table 10. Onc can clearly see that for each terminal time T the error decays as the grid resolutions increase. Notice that for this problem the wave functions $u^{(1)}$ and $u^{(2)}$ are continuous at the interface but the derivatives of them along the direction normal to the interface are discontinuous. A snapshot of the computed field provided in Fig. 11 illustrates this feature at the interface $r = 2.5$.

4. Concluding Remarks

In this study we proposed a high-order accurate numerical scheme for solving the second-order wave equation in curvilinear coordinates. The scheme is based on a Legendre pseudospectral penalty method in

Table 10: Convergence study results for Example 5. The terminal time T is measured in terms of the fundamental period in time $p = 1.816858313802119$. N_r and N_θ are grid resolutions in radial and azimuthal direction within each subdomain. $\gamma = 1.1$

		$T = 1p$		$T = 10p$		$T = 100p$	
N_r	N_θ	$e(N)$	q	$e(N)$	q	$e(N)$	q
6	9	1.5774e-03	-	1.7655e-03	-	1.5774e-03	-
8	12	2.3758e-05	7.29	2.4378e-05	7.44	2.3758e-05	7.29
10	15	1.2321e-07	11.79	1.2443e-07	11.82	1.2321e-07	11.79
12	18	2.8065e-09	10.37	3.4813e-09	9.80	2.8065e-09	10.37

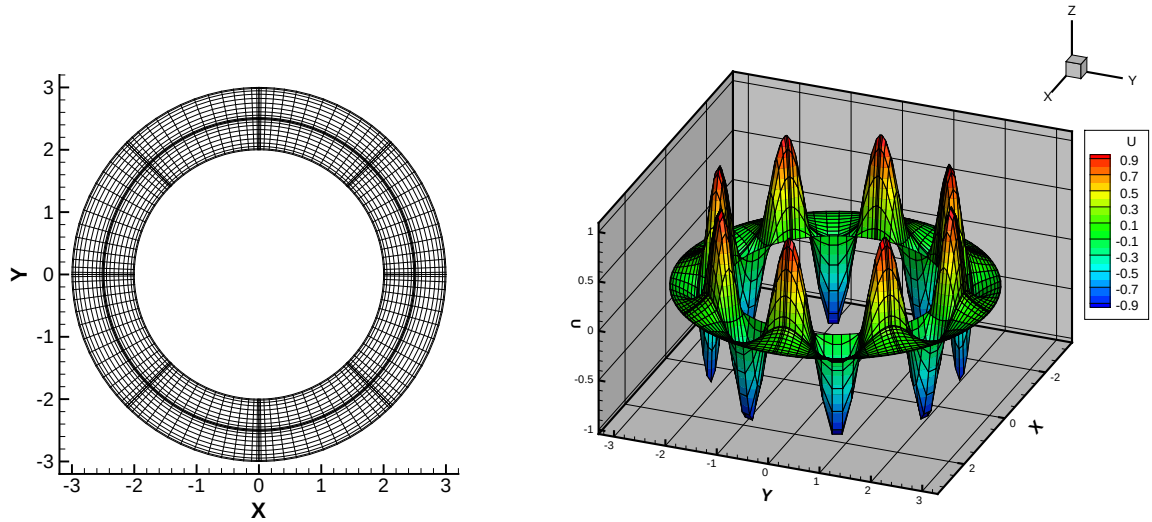

Figure 11: Left: Multidomain mesh for simulating waves in a ring waveguide. Right: Computed wave field at $T = 10p$.

space and a Runge-Kutta-Nyström method in time. To ensure stable computations, we conducted discrete energy estimates in order to determine suitable penalty parameters for problems subject to different types of boundary conditions. In addition, we propose an accuracy-consistent approach for imposing boundary conditions at the RKN intermediate stages to avoid accuracy order reduction. To validate the method, we conducted numerical experiments for various problems, and we observe the expected convergence rate.

The present method is for the scalar wave equation. We plan to extend the method for systems of wave equations in second-order forms such as vectorial wave equations resulting from raising the order of the Maxwell equations in electromagnetic or the elastic wave equations.

Acknowledgements

This work is supported in part by National Science Council of Taiwan under grant NSC99-2115-M-009-012-MY3. The author Chun-Hao Teng is supported by the National Science Council of Taiwan under Research Fellow Program NSC099-2811-M-009-47. Misun Min is supported by the U.S. Department of Energy, under Contract DE-ACO2-O6CH11357.

References

[1] C. Agut, J. Diaz, A. Ezziani, High-order schemes combining the modified equation approach and discontinuous Galerkin approximations for the wave equation, Commun. Comput. Phys. 11 (2012) 691-708.

[2] P. F. Antonietti, I. Mazzieri, A. Quarteroni, F. Rapetti, Non-conforming high order approximations of the elastodynamics equation, Comput. Methods Appl. Mech. Engrg. 209-212 (2012) 212-238.

[3] D. Appelo, N. A. Petersson, A stable finite difference method for the elastic wave equation on complex geometries with free surfaces, Commun. Comput. Phys. 5 (2009) 84-107.

[4] M. Baccouch, A local discountinuous Galerkin method for the second-order wave equation, Comput. Methods Appl. Mech. Engrg. 209-212 (2012) 129-143.

[5] M. H. Carpenter, D. Gottlieb, S. Abarbanel, W. S. Don, The theoretical accuracy of Runge-Kutta time discretizations for the initial boundary value problem: A study of the boundary error, SIAM J. Sci. Comput. 16 (1995) 1241-1252.

[6] K. Duru, G. Kreiss, A well-posed and discretely stable perfectly matched layer for elastic wave equations in second order formulation, Commun. Comput. Phys. (2012) 11 1643-1672.

[7] E. Faccioli, F. Maggio, R. Paolucci, A. Quarteroni, 2D and 3D elastic wave propagation by a pseudo-spectral domain decomposition method, J. of Seismol. 1 (1997) 237-251.

[8] S. E. Field, J. S. Hesthaven, S. R. Lau, A. H. Mroue, Discontinuous Galerkin method for the spherically reduced BSSN system with second-order operators, Physical Review D 82 (2012) 104051.

[9] K. A. Feng, M. H. Teng, M. H. Chen, A Legendre pseudospectral penalty scheme for 2D isotropic elastic wave computations, J. Sci. Comput. 33 (2007) 313.

[10] D. Funaro, D. Gottlieb, A new method of imposing boundary conditions in pseudospectral approximations of hyperbolic equations, Math. Comp. 51 (1988) 599-613.

[11] D. Funaro, D. Gottlieb, Convergence results for pseudospectral approximations of hyperbolic systems by a penalty-type boundary treatment, Math. Comp. 57 (1991) 585-596.

[12] A. Gelb, Z. Jackiewicz, B. D. Welfert, Absorbing boundary conditions of the sceond order for the pseudospectral Chebyshev methods for wave propagation, J. Sci. Comput. 17 (2002) 501-512.

[13] D. Gottlieb, M. Gunzburger, E. Turkel, On numerical boundary treatment of hyperbolic systems for finite difference and finite element methods, SIAM J. Numer. Anal. 19 (1982) 671-682.

[14] W. J. Gordon, C. A. Hall, Transfinite element methods: Blending-function interpolation over arbitrary curved element domains, Numer. Math. 21 (1973) 109-129.

[15] W. J. Gordon, C. A. Hall, Construction of curvilinear co-ordinate systems and applications to mesh generations, Int. J. Numer. Meth. Eng. 7 (1973) 461-477.

[16] M. Grote, A. Schneebeli, D. Schötzau, Discontinuous Galerkin finite element method for the wave equations, SIAM J. Numer. Anal. 44 (2006) 2408-2431.

[17] M. Grote, A. Schneebeli, D. Schötzau, Interior penalty discontinuous Galerkin method for Maxwell's equations: Energy norm error estimates, J. Comput. Appl. Math. 204 (2007) 375-386.

[18] C. Gundlach, J. M. Martín-García, Symmetric hyperbolic form of systems of second-order evolution equations subject to constraints, Phys. Rev. D 70 (2004) 044031.

[19] C. Gundlach, J. M. Martín-García, Hyperbolicility of second order in space systems of evolution equations, Class. Quant. Grav. 23 (2006) S387.

[20] J. S. Hesthaven, A stable penalty method for the compressible Navier–Stokes equations: III. multidimensional domain decomposition schemes, SIAM J. Sci. Comput. 20 (1998) 62-93.

[21] J. S. Hesthaven, Spectral penalty methods, Appl. Numer. Math. 33 (2000) 23-41.

[22] J. S. Hesthaven, T. Warburton, Nodal high-order methods on unstructured grids: I. time-domain solution of Maxwell's equations, J. Comput. Phys. 181 (2002) 186-221.

[23] J. S. Hesthaven, S. Gottlieb, D. Gottlieb, Spectral Methods for Time-Dependent Problems, Cambridge University Press, Cambridge, UK, 2007.

[24] D. Komatitsch, J. Tromp, Introduction to the spectral element method for three-dimensional seismic wave propagation, Geophys. J. Int. 139 (1999) 806-822.

[25] D. Kondaxakis, S. Tsangaris, Pseudospectral solution of linear evolution equations of second order in space and time on unstrutured quadrilateral subdomain topologies, J. Comput. Phys. 202 (2005) 537-576.

[26] H. O. Kreiss, J. Oliger, Comparison of accurate methods for integration of hyperbolic equations, Tullus 24 (1972) 3.

[27] H. O. Kreiss, N. A. Petersson, J. Ystrom, Difference approximations for the second order wave equation, SIAM J. Numer. Anal. 40 (2002) 1940-1967.

[28] K. Mattsson, Summation by parts operators for finite difference approximations of second-derivatives with variables coefficients, J. Sci. Comput. 51 (2012) 650-682.

[29] K. Mattsson, J. Nordström, Summation by parts operators for finite difference approximationsof second deverivatives, J. Comput. Phys. 199 (2004) 503-540.

[30] K. Mattsson, J. Nordström, High order finite difference methods for wave propagation in discontinuous media, J. Comput. Phys. 220 (2006) 249-269.

[31] K. Mattsson, F. Ham, G. Iaccarino, Stable and accurate wave-propagation in discontinuous media, J. Comput. Phys. 227 (2008) 8753-8767.

[32] K. Mattsson, F. Ham, G. Iaccarino, Stable boundary treatment for the wave equation on second-order form, J. Sci. Comput. 41 (2009) 366-383.

[33] K. Mattsson, F. Parisi, Stable and accurate second-order formulation of the shifted wave equation, Commun. Comput. Phys. 7 (2010) 103-137.

[34] E. J. Nyström, Über die numerische Integration von Differentialgleichungen, Acta Soc. Sci. Fenn. 50 (1925) 1

[35] R. Renaut, J. Frohlich, A pseudospectral Chebyshev method for the 2D wave equation with domain stretching and absorbing boundary conditions, J. Comput. Phys. 124 (1996) 324-336.

[36] B. Sjógreen, N. A. Petersson, A fourth order accurate finite difference scheme for the elastic wave equation in second order formulation, J. Sci. Comput. 52 (2012) 17-48.

[37] N. W. Taylor, L. E. Kidder, S. A. Teukolsky, Spectral methods for the wave equation in second-order form, Physical Review D 82 (2012) 024037.

[38] C. H. Teng, B. Y. Lin, H. C. Chang, H. C. Hsu, C. N. Lin, K. A. Feng, A Legendre pseudospectral penalty scheme for solving time-domain Maxwells equations, J. Sci. Comput. 36 (2008) 351-390.

[39] J. Tromp, D. Komatitsch, Q. Liu, Spectral-element and adjoint methods in seismology, Commun. Comput. Phys. 3 (2008) 1-32.